Title

N6-methyladenosine modification and the YTHDF2 reader protein play cell type specific roles in lytic viral gene expression during Kaposi’s sarcoma-associated herpesvirus infection

Author

Hesser, Charles

Publication Date

2018

Peer reviewed|Thesis/dissertation

N^6-methyladenosine modification and the YTHDF2 reader protein play cell type specific roles in lytic viral gene expression during Kaposi's sarcoma-associated herpesvirus infection

By

Charles Hesser

A dissertation submitted in partial satisfaction of the

Requirements for the degree of

Doctor of Philosophy

in

Molecular and Cell Biology

in the

Graduate Division

of the

University of California, Berkeley

Committee in charge:

Professor Britt A. Glaunsinger, Chair
Professor Laurent Coscoy
Professor Qiang Zhou
Professor Danica Chen

Fall 2018

Abstract

N^6-methyladenosine modification and the YTHDF2 reader protein play cell type specific roles in lytic viral gene expression during Kaposi's sarcoma-associated herpesvirus infection

By Charles Hesser

Doctor of Philosophy in Molecular and Cell Biology

University of California, Berkeley

Professor Britt A. Glaunsinger, Chair

More than 100 types of RNA modifications are known to exist, regulating key aspects of cellular biology and metabolism. First discovered to be present on viral RNAs in the 1970s, methylation at the N^6 position of adenosine (m^6A) is the most abundant internal modification within eukaryotic mRNAs, and is proposed to be dynamically regulated during times of cellular stress. However, the transcriptome-wide distribution and function of m^6A in the lifecycle of a dsDNA virus had not been explored. In Chapter 1, I review how human herpesviruses manipulate host pathways in order to replicate, with particular emphasis on gammaherpesviruses. I also discuss the diverse roles played by RNA modifications in gene expression, focusing on enzymes that install m^6A (writers), and proteins that bind m^6A modified mRNA (readers). In Chapter 2, I present a detailed investigation of how the m^6A pathway impacts the lifecycle of the oncogenic human virus Kaposi's sarcoma-associated herpesvirus (KSHV). Mass spectrometry and transcriptome-wide m^6A-sequencing revealed enrichment of m^6A in viral transcripts upon lytic reactivation, including in the lytic transactivator ORF50. Depletion of the writer METTL3 and reader YTHDF2 in three different KSHV reactivation models had differential pro- and anti-viral impacts on viral gene expression depending on the cell-type analyzed. Finally, in Chapter 3, I put my findings in the broader context of the literature examining m^6A modifications in viral lifecycles. I discuss technical challenges that have hindered research to-date, and potential reasons for the diverse pro and anti-viral effects ascribed to the m^6A pathway, including a discussion of why the m^6A pathway may have cell-type specific effects. I highlight the impact of m^6A deposition on host transcripts, including those of the innate immune system. Overall, this study demonstrates the critical importance of m^6A modifications in regulating KSHV lytic gene expression and sets the stage for future studies to elucidate more mechanistic details, including the potential for discrete impacts at different stages of the viral lifecycle.

TABLE OF CONTENTS

List of Figures and Tables

List of Symbols and Abbreviations

RNA Modification Pathway	
N^6-methyladenosine	m^6A
N^1-methyladenosine	m^1A
Pseudouridine	ψ
5-methylcytidine	m^5C
Methyltransferase like 3	METTL3
Methyltransferase like 14	METTL14
WT1 associated protein	WTAP
Methyltransferase like 16	METTL16
YTH N^6-methyladenosine RNA binding protein 1	YTHDF1
YTH N^6-methyladenosine RNA binding protein 2	YTHDF2
YTH N^6-methyladenosine RNA binding protein 3	YTHDF3
YTH domain containing 1	YTHDC1
YTH domain containing 2	YTHDC2
AlkB homolog 5, RNA demethylase	ALKBH5
FTO, alpha-ketoglutarate dependent dioxygenase	FTO
Insulin-like growth factor 2 mRNA binding proteins	IGFBP1-3
Heterogeneous nuclear ribonucleoprotein C (C1/C2)	HNRNPC
RNA binding motif protein X-linked	HNRNPG/RBMX
Heterogeneous nuclear ribonucleoprotein A2/B1	HNRNPA2B1
Viruses	
Kaposi's sarcoma-associated herpesvirus	KSHV
Murine gammaherpesvirus 68	MHV-68
Epstein-Barr virus	EBV
Mouse cytomegalovirus	MCMV
Human cytomegalovirus	HCMV
Herpes simplex virus type 1	HSV-1
Simian virus 40	SV40
Influenza A virus	IAV
Hepatitis B virus	HBV
Human immunodeficiency virus	HIV
Hepatitis C virus	HCV
KSHV cell lines and gene names	
r.219 KSHV infected renal carcinoma cell line	iSLK.219
BAC16 KSHV infected renal carcinoma cell line	iSLK.BAC16
KSHV-positive body-cavity-based lymphoma cell line	TREX-BCBL-1
Replication and transcription activator	RTA/ORF50
RTA-responsive element	RRE
Latency-associated nuclear antigen	LANA/ORF73

Acknowledgments

I want to thank everyone in the Glaunsinger Lab for helpful feedback and support throughout my Ph.D. In particular, I want to thank Britt from being the best mentor anyone could hope to have: always engaged, respectful, focused, organized and supportive. In addition, I want to thank my rotation mentor Zoe Davis, who was instrumental in my training, and John Karijolich for his guidance and expertise in RNA modifications. I also want to thank my thesis committee, in particular Laurent for many helpful discussions, and my terrific MCB 2013 classmates!

Chapter 1: Introduction

Section I: Herpesviridae

The *Herpesviridae* are double-stranded DNA viruses that infect a wide range of organisms and are distinguished from other DNA viruses by their ability to establish lifelong infections. In terms of their architecture, herpesviruses feature an icosahedral capsid which packages and protects the viral DNA, and an outer lipid envelope derived from the host membrane studded with glycoproteins[1]. In between the envelope and capsid is the tegument, which consists of viral RNA and protein. The components of the tegument are thereby directly released into the host cell upon *de novo* infection, and can immediately modulate host functions. The size of mature herpesviruses ranges from 120 to 300 nm, as the size of the viral tegument is variable[1]. One of the most distinctive features about herpesviruses is their biphasic lifecycle. Herpesviruses are able to persist in a latent or quiescent state upon infecting a host cell. Unlike retroviruses, herpesviruses do not integrate into the host DNA. Instead, the viral genome persists as a collection of episomes, which are passively replicated by the host DNA polymerase each time the cell divides. The viral episomes are rapidly chromatinized and gene expression is tightly restricted. Upon cellular stress, the lytic cycle is induced, consisting of a temporally regulated, ordered cascade of viral gene expression. Each stage of the viral lifecycle leads to the next, ensuring that the necessary viral proteins are available as they are required. Immediate early genes are produced, which include viral activators of transcription, followed by delayed early genes, which encode components of the viral DNA replicase. Next, the viral DNA is replicated, which in turn licenses late gene expression. Late genes primarily consist of capsid proteins and envelope glycoproteins. Newly synthesized viral genomes are loaded into viral capsids in the nucleus, which then bud through the nuclear membrane to acquire the envelope[1].

The family *Herpesviridae* is divided into three subfamilies: *alphaherpesvirinae, betaherpesvirinae,* and *gammaherpesvirinae*. All of these subfamilies comprise highly seroprevalent human pathogens[1]. *Alphaherpesvirinae* were the first to be characterized and are thus among the best studied. These viruses are neurotropic, first infecting epithelial cells, but then establishing latency in sensory ganglia. These viruses induce extensive cytoskeletal rearrangement and co-opt the host axonal transport mechanisms to travel between the epithelial surface and the ganglion. The three human herpesviruses in this subfamily are Herpes Simplex Virus-1 (HSV-1), which causes cold sores, HSV-2 which causes genital warts, and Varicella Zoster Virus (VZV), which causes chicken pox. Compared to other subfamilies, *alphaherpesvirinae* exhibit faster replicative kinetics, although the stages of gene expression are the same as in other subfamilies. *Betaherpesvirinae* include human cytomegalovirus (HHV-5), HHV-6 and HHV-7. These viruses can infect epithelial cells, leukocytes and lymphocytes[1]. HHV-5 can cause mononucleosis, as well as severe birth defects when contracted during pregnancy due to its ability to be horizontally transmitted. HHV-6 and HHV-7 are common causes of childhood rashes[1]. Among *gammaherpesvirinae*, both Epstein Barr Virus (EBV) and Kaposi's Sarcoma Herpesvirus (KSHV) infect humans. These viruses are lymphotropic and can cause a variety of cancers and diseases as described below.

Gammaherpesviruses

EBV is highly prevalent in the adult human population. For most individuals, EBV is encountered during childhood and is either asymptomatic or results in symptoms indistinguishable from the common cold. It is the primary cause of infectious mononucleosis, but can also lead to lymphoblastoid diseases, including Burkitt's lymphoma, nasopharygeal carcinoma and Hodgkin's lymphoma [2]. The virus infects epithelial cells and then spreads to adjacent B cells. Although robust NK and CD8 T cell responses will greatly restrict viral replication, the virus still establishes latency in memory B cells [1]. More so than in other herpesviruses, EBV latency consists of a very complex pattern of gene expression designed to prolong the lifespan of the B cell while evading immune detection [1]. Although the virus periodically reactivates in mucosal tissues, the CD8 T cell response will kill infected cells. However, the transformation of B cells latently infected with EBV can lead to cancer.

KSHV (HHV-8) is the etiologic agent of primary effusion lymphoma (PEL), multicentric Castleman's disease, and the AIDS-associated neoplasm Kaposi's sarcoma[3]. Most people infected with KSHV are asymptomatic, but in AIDS patients, immunosuppression leads to characteristic KS blood vessel lesions visible on the surface of the skin[4]. KSHV seroprevalence is highest in sub-Saharan Africa, although it is also common amongst elderly Mediterranean men[5]. While Moritz Kaposi first characterized these lesions in 1872, it is was not until 1994 that HHV-8 was discovered to be its causative agent. Perhaps owing to its more recent discovery with respect to other herpesviruses, the functions of many KSHV proteins have yet to be characterized. Bounded on either end by terminal repeats, the viral genome is 170 kB in length and contains two lytic origins of replication. During the lytic cycle, around 90 KSHV ORFs are expressed, as well as the abundant viral lncRNA PAN.

Like all herpesviruses, KSHV genes are expressed in a temporally regulated, ordered cascade. Given the complexity of the KSHV lifecycle, the virus relies heavily on host processes to complete its lytic cycle. The default state of the virus is latency, in which a multicistronic latency associated transcript is expressed, as well as a cluster of viral microRNAs[3]. These proteins contribute to transforming the host cell environment and maintaining the viral genome. Of particular importance is ORF73, also called Latency Associated Nuclear Antigen (LANA), which tethers the viral DNA to host chromatin. Upon cellular stress, ORF50, also called RTA, is transcribed. RTA expression is necessary and sufficient for lytic reactivation [6-8]. RTA directly transactivates its own promoter, as well as those of downstream viral genes containing an RRE, or RTA-responsive element. However, for some viral transcripts, direct interaction between RTA and the cellular co-factor RBK-jk is required for transactivation[3]. In addition, other cellular co-factors such as C/EBPα, C-Jun, and SP1 play a role in RTA-mediated gene expression. RTA acts at early promoters, while late gene promoters are instead bound by different viral transactivator, ORF24 [9]. Upon promoter activation, a transcription pre-initiation complex forms which includes canonical general transcription factors (GTFs) and the host RNA Polymerase II. Analogous to cellular mRNAs, KSHV mRNAs are co-transcriptionally modified via 5' capping, splicing and polyadenylation. While the basic mechanisms of viral transcription and mRNA processing have been examined, one area that had not been studied is the involvement of host mRNA modifying enzymes in viral gene expression. KSHV relies on

host processes which are in turn subject to extensive regulation by internal mRNA modifications. Given that mRNA modifications have been proposed to play a role in cancer and immune responses, we hypothesized that this could represent a new regulatory axis for viral mRNA [10-12].

Section II: RNA Modifications

The post-transcriptional control of mRNA, including its splicing, nuclear export, and decay, is critical to managing the amplitude and duration of gene expression. Owing to the inherent instability of RNA compared to DNA, the cell must devise mechanisms to sense mRNA abundance and carefully regulate its homeostasis. While the basic mechanisms of mRNA processing have been well studied, emerging evidence shows that covalent chemical modifications play a critical role in fine-tuning the mRNA lifecycle [10,13,14]. Indeed, the most abundant mRNA modification is the 7-methylguanosine cap (m^7G), which contains a reverse 5'-to-5' triphosphate linkage. Not only does the cap play a critical role in preventing mRNA degradation, but it also recruits the eukaryotic translation initiation factor 4E (eIF4E) to enable translation initiation [13,14]. Subsequent work in the 1970s and 1980s revealed that internal base modifications play critical roles in the processing and maturation of mRNA, tRNA and rRNA. These modifications include pseudouridine, 5-methylcytidine, N^1-methyladenosine, and N^6-methyladenosine [10,13-16]. Until recently, technological barriers to the systematic study of RNA modifications prevented detailed analysis of their function. Thanks to recent advancements in high throughput sequencing, RNA immunoprecipitation (RIP) technology, and antibody specificity, accurate transcriptome-wide mapping of several RNA modifications now exists [15-18]. Today, more than 140 types of RNA modifications are known, and the functional consequences of these modifications are just beginning to be explored [13,14]. Generally speaking, the enzymes that install RNA modifications are known as writers, while readers act as selective binding proteins for modified RNA, helping to direct the modified RNAs to specific protein complexes in the cell. Finally, for modifications that are reversible, erasers are enzymes that serve to remove the modification.

Pseudouridine (ψ)

ψ is found in small nuclear RNAs, rRNA and mRNA[19]. The isomerization of uridine, in which the base is rotated 180 degrees, does not alter Watson-Crick base-pairing but does result in an additional hydrogen bond donor. The addition of ψ to RNA makes the phosphodiester backbone more rigid and enhances the thermodynamic stability of ψ-A base pairs. In eukaryotes, U-to- ψ isomerization can occur in either an RNA-dependent or RNA-independent fashion [20]. In the RNA-independent mode, a single pseudouridine synthase (PUS) enzyme caries out both substrate recognition and catalysis. In the RNA-dependent mode, H/ACA noncoding RNAs in conjunction with the Cpf5/Dyskerin protein complex lead to its deposition[19]. A method using N-cyclohexyl-N'-beta-(4-methylmorpholinium)ethylcarbodiimide p-tosylate (CMCT) chemical labeling revealed hundreds of ψ sites in yeast and human mRNAs [17,21]. ψ is found throughout coding regions, and is believed to represent between 0.2 and 0.6% of total uridines [22]. GUψC and UGψAG motifs are reported as consensus motifs in humans[13]. ψ is thought to be induced by conditions of cellular stress, but has not been shown to be reversible [13]. One clear phenotype for ψ is translational regulation through recoding.

For example, isomerization of U to ψ in nonsense codons suppresses translation termination in vitro and in vivo [23]. Thus, pseudouridine has considerable potential to alter the translational landscape during conditions of cellular stress.

N^1-methyladenosine (m^{1}A)

m^{1}A is installed by methyltransferases TRMT6/TRMT61A, TRMT61B and TRMT10C and removed by the demethylases ALKBH1, ALKBH3 and FTO [13,24]. In addition to mRNA, m^{1}A exits in transfer RNA (tRNA) and rRNA and is unique in that it has both a methyl group and a positive charge under physiological conditions[25]. Two high throughput studies revealed the presence of numerous m^{1}A modified human and mouse mRNAs, with a high degree of conservation between species [26,27]. These studies failed to find a clear consensus motif, although one study found enrichment in GC-rich and structured regions in the 5'UTR[27]. Mapping techniques have relied on immunoprecipitation using a m^{1}A specific antibody and the inherent ability of m^{1}A to stall reverse transcription. The relative m^{1}A/A ratio in mRNA is reported at about 0.02%, making it a relatively low abundance modification [26]. The function of m^{1}A is not well understood, although its presence is positively correlated with translational efficiency and protein levels [25,27]. YTHDF proteins were recently reported to serve as readers for m^{1}A, in addition to their role in recognizing *N*^{6}-methyladenosine [28]. m^{1}A is reported to be dynamically regulated during times of cellular stress, and expression levels vary by tissue [13,25,27].

5-methylcytidine (m^{5}C)

m^{5}C is common modification in DNA that has recently been demonstrated to exist in mRNA as well. Indeed, while m^{5}C promoter methylation in DNA is an important mechanism to regulate gene expression, its function in mRNA is less clear. An initial experimental approach using bisulfite sequencing demonstrated the presence of thousands of modification sites throughout mRNAs and ncRNAs [29,30] [31]. However, a subsequent approach using a chemical analogue of cytidine (5-azacytidine) revealed only several hundred m^{5}C sites [32]. The conditions required for bisulfite sequencing may not be conducive to RNA owing to its reduced stability compared to DNA [13]. NSUN1-7 and DNMT2 have all been proposed to act as m^{5}C methyltransferases in human cells[32]. Among these, NSUN2 appears to have the broadest substrate specificity, methylating tRNAs, mRNAs and some noncoding RNAs [13]. A recent study proposed that ALYREF acts as a m^{5}C reader [15]. ALYREF is a component of the cellular TREX complex important for mRNA export, and thus m^{5}C is implicated in nuclear export of mRNA. The m^{5}C modification can undergo oxidation to form 5-hydroxymethylcytidine via the enzyme Tet2, although it has not been shown to be completely reversible[15,25]. In summary, while m^{5}C is likely an abundant mRNA modification, technical challenges in mapping m^{5}C sites and the presence of multiple methyltransferases render this modification challenging to study.

N^6-methyladenosine (m^{6}A)

Among internal mRNA modifications, m^{6}A quickly emerged as a compelling and accessible target for transcriptome-wide study. First of all, m^{6}A is the most abundant internal mRNA modification, occurring at a stoichiometry of 1-2 per 1000 bp, and has

been shown to play an essential role in embryonic development in multiple organisms [13,14,16,33,34]. Second, both the enzymes responsible for m^6A deposition and their consensus motif are known, enabling global analysis of the effects of m^6A on gene expression through methyltransferase depletion [16,35-38]. Furthermore, introduction of a synonymous mutation into a locus containing the m^6A consensus motif could potentially serve as a way deplete m^6A in a site-specific manner [39-41]. Third, a technique known as m^6A-seq has coupled immunoprecipitation of m^6A containing transcripts to deep-sequencing, enabling transcriptome-wide identification of m^6A sites [16]. Fourth, several papers have indicated dramatic changes in the m^6A profile during times of cellular stress, including the appearance of m^6A sites in the 5' UTR of transcripts that facilitate cap-independent translation [42,43]. For all of these reasons, interest in the m^6A modification has burgeoned in recent years. However, an understanding of m^6A function requires thorough analysis of the proteins that add, decode and remove m^6A.

Section III: m^6A-mediated gene expression

Writers

The m^6A methyltransferase consists of a heterodimeric complex of METTL3, METTL14 as well as several other accessory proteins including WTAP and KIAA1429. Addition of m^6A occurs co-transcriptionally, with modifications deposited near splice junctions and introns, as well as throughout long internal exons and UTRs. The catalytic subunit, METTL3, utilizes S-Adenosyl Methionine (SAM) as the methyl donor, and catalyzes the addition of m^6A at a broad consensus motif of RRACH, where R represents G or A and H = A, C, or U, with the strongest enrichment for GGAC [14,35,44]. METTL14 contains a methyltransferase domain, but is catalytically inactive, instead helping METTL3 achieve proper substrate specificity [35]. WTAP acts as a scaffold protein mediating the localization of METTL3-METTL14 to nuclear speckles, while KIAA1429 has been implicated in methylation at the 3'UTR and is associated with polyadenylation factors CPSF5 and CPSF6 [11,45,46]. While the nuclear speckles are thought to be the primary site of mRNA modification, cytoplasmic localization of METTL3 and addition of m^6A has been reported in some cell types [41,47,48]. Interestingly, the RRACH motif occurs every 86th nucleotide on the transcript on average, far in excess of the actual periodicity of m^6A deposition[25]. Even on transcripts that are methylated, the stoichiometry of modification at any given RRACH motif is highly variable. Determining what governs the extent to which a particular m^6A consensus motif is methylated requires future investigation.

Additional functions of METTL3 are the subject of active research. METTL3 is subject to post-translational modifications, such as sumoylation, although how they impact METTL3 function remains to be fully elucidated [36]. Extending beyond its catalytic role, METTL3 can directly enhance translation in a lung adenocarcinoma cell line by binding to the 5' UTR of methylated transcripts, promoting growth survival and invasion of tumor cells[49]. A recent study showed that physical interaction between METTL3 and the translation initiation factor eIF3h led to circularization and increased translation of mRNAs, including oncogenic mRNAs that are m^6A modified

[50]. Thus, in addition to reducing m^6A deposition, depletion of METTL3 may also impair translation of modified transcripts in transformed cell lines.

Another methyltransferase, METTL16, has recently been implicated in deposition of m^6A. Although METTL16 has been far less extensively studied than METTL3, m^6A deposition by METTL16 is thought to involve a combination of sequence and structure [51,52]. Like METTL3/14, the methyl donor is SAM. However, unlike the heterodimeric METTL3/14 complex, METTL16 is thought to be monomeric based on size-exclusion chromatography [52]. The U6 snRNA has long been known to be m^6A modified, but until recently, the methyltransferase responsible was unknown [51]. METTL16 catalyzes the addition of m^6A to structured RNAs carrying a specific nonamer sequence of UAC**m^6A**GAGAA [51]. During methionine starvation, cells induce MAT2A expression, which regulates the SAM synthetase. Intron retention of the SAM synthetase MAT2 mRNA is responsive to levels of SAM[51]. In both HeLa cells and mouse embryos, METTL16 writes m^6A onto a conserved hairpin in the *MAT2A* 3' UTR, indicating this mechanism is conserved across species [51] [53]. Thus, while METTL3/14 is responsible for the majority of m^6A distribution on mRNAs, METTL16 can also add m^6A to certain structured regions of mRNA and also to the U6 snRNA.

Erasers

Two proteins have been identified as putative m^6A erasers: FTO and ALKBH5. FTO belongs to the superfamily of Fe(II) 2-oxoglutarate dependent oxygenases, and mutations in FTO are associated with gain in human body weight [54-57]. ALKBH5 was shown to be important for mouse fertility, as mice deficient in ALKBH5 have shrunken testes [58]. While originally proposed to function in a similar manner, recent studies have suggested that FTO and ALKBH5 have different substrate specificities. ALKBH5 demethylates transcripts containing m^6A, including viral transcripts [47,58]. However, FTO has greater substrate specificity *in vitro* and *in vivo* for the 5' cap-adjacent nucleotide containing *N^6*- methyladenosine*, 2'O*-methylation (m^6Am), which occurs on about 10% of transcripts [59]. This m^6Am modification is thought to enhance transcript stability by providing resistance to decapping mediated by DCP2 [13,59]. However, other studies show FTO can effectively demethylate m^6A from mRNAs [54,60]. Furthermore, the observation that FTO depletion strongly impacts Hepatitis C virus (HCV) virion formation suggests that FTO does not only act on m^6Am, as HCV RNA contains m^6A but not m^6Am [13,41]. Thus, future studies are required to analyze the substrate specificity of FTO across cell types.

YTH-domain reader proteins

The first-identified and best studied class of m^6A readers are the YTH domain binding proteins. A conserved, key feature of these proteins is the C-terminal YTH domain, which contains a conserved aromatic cage required for binding m^6A containing mRNA [11,61]. Crosslinking Immunoprecipitation and Sequencing (CLIP-seq) studies have revealed that YTHDF proteins primarily target the GGAC m^6A consensus motif [61-64]. Among these readers, YTHDF2 has been most extensively studied. YTHDF2 has been shown to destabilize transcripts containing m^6A in their 3'UTRs and remove them from the translatable pool [61]. These transcripts have a notably increased half-life in HeLa cells upon depletion of YTHDF2. This likely occurs

because the N-terminal P/Q/N-rich domain of YTHDF2 recruits the CCR4-NOT adenylase complex through direct interaction between the SH domain of CNOT1, leading to deadenylation of transcripts containing m^6A sites in their 3' UTRs [66]. Furthermore, YTHDF1 and 3 were shown to promote the same effect to a slightly lesser degree[66]. It should be noted that these studies were carried out in HeLa or HEK293 cells, thus raising questions about their broader applicability to primary cells and other types of cancer cell lines. For example, a study examining acute myeloid leukemia revealed that YTHDF2 depletion had no impact on m^6A modified transcript levels [67]. Thus, YTHDF2 may only mediate mRNA degradation in certain cell types.

Less well studied are the other closely related paralogs, YTHDF1 and 3. Along with YTHDF2, these readers show similar, although not identical patterns of binding to m^6A modified transcripts in CLIP-seq studies. In addition to its role in mRNA decay, YTHDF1 has been shown to bind transcripts containing m^6A in their 3' UTR, recruiting eIF3 and the 40s ribosomal subunit in HeLa cells. In this manner, YTHDF1 binding directly elevates translation efficiency of 5' capped transcripts [62]. YTHDF1 has not been shown to have this function in HEK293 cells, although a role in translation of axonal neurons has been suggested [68]. YTHDF3 has been proposed to assist in the function of YTHDF1 in promoting translation and YTHDF2 in promoting mRNA decay[63,64]. Purified YTHDF3 interacts with ribosomal proteins and the RNA binding affinity of YTHDF3 increases upon depletion of YTHDF1 and vice versa [64]. Thus, the YTHDF proteins may function cooperatively to some extent, in addition to potentially having independent functions.

Recently, several studies have emerged characterizing the functions of a nuclear reader, YTHDC1[69-72]. m^6A has been suggested to play a role in splicing, as methylation inhibitors led to the accumulation of some modified, unspliced pre-mRNAs [13]. YTHDC1 has been shown to promote splicing of modified transcripts by binding to m^6A and forming a complex with SRSF3. SRSF3, in turn, binds exons containing m^6A modifications, thus leading to exon inclusion [69]. At the same time, YTHDC1 antagonizes SRSF10, which would normally lead to exon skipping. In HeLa cells, depletion of YTHDC1 results in nuclear accumulation of methylated mRNAs [73]. In addition, it has been proposed that YTHDC1 plays a role in processing mature mRNAs that lack introns and that it may shuttle between the nucleus and the cytoplasm [51,74]. In support of YTHDC1 playing a role in nuclear mRNA, a recent study revealed YTHDC1 interacts with the TREX mRNA export complex [72]. The methyltransferase complex recruits TREX to m^6A modified mRNAs, which in turn stimulates recruitment of the m^6A reader protein YTHDC1 to the mRNA to promote export. Additionally, loss of YTHDC1 has been shown to alter 3' UTR length in oocytes and is correlated with alternative polyadenylation [70]. Thus, YTHDC1 appears to play a role in multiple components of the processing of m^6A modified mRNAs.

The fifth YTH reader, YTHDC2, has only been recently characterized and is structurally distinct from the other family members. Unlike the other YTH domain proteins, YTHDC2 contains a 3'→5' RNA helicase/ATPase domain in addition to its YTH domain [75,76]. YTHDC2 was shown to be highly expressed in testes, and important for spermatogenesis and meiotic prophase I [76]. Two functions have been proposed: promoting mRNA decay through recruitment of 5'→3' exoribonuclease XRN1 in mouse male germ line cells, and recruiting the small ribosomal subunit to increase translation

[75,76]. So far, it is not understood what determines whether YTHDC2 augments the translation or decay of a given transcript. However, these functions are consistent with m^6A modification being important in the context of both mRNA decay and translation initiation.

IGFBP reader proteins

The insulin-like growth factor 2 mRNA binding proteins (IGFBP1, IGFBP2, IGFBP3) bind to m^6A containing mRNA through RRM and KH domains, and thus bind mRNA through a mechanism distinct from the YTH-domain proteins [77]. Importantly, as IGFBP binding is reported to enhance the stability of modified transcripts, it follows that the m^6A modification can either increase or decrease transcript stability depending on the reader protein present. Given that IGFBPs target the same m^6A consensus motif as YTH-domain proteins, how any given reader is recruited to a specific m^6A site remains unknown [61,62,77]. Interestingly, only about 30% of IGFBP targets overlap with YTHDF2 targets [78]. Thus, an intriguing regulatory scenario could exist in which different reader "families" target distinct pools of transcripts to exert differential effects on their stability. As IGFBP proteins were only recently characterized as readers, additional studies will be required to analyze their function across cellular contexts.

Indirect and structure-dependent reader proteins

While the aforementioned families of readers recognize RNA in a sequence-dependent manner, an additional family of structure-dependent m^6A readers also exists. These so-called "indirect readers" do not directly bind m^6A through a hydrophobic domain. Instead, the presence of m^6A in a hairpin region alters the secondary structure of the mRNA and enables an RNA binding protein to bind to a nearby motif. For example, HNRNPC belongs to family of heterogeneous nuclear ribonucleoproteins that bind nascent mRNA transcripts and impact their stability, splicing, and export[79-81]. HNRNPC binds single-stranded U-rich tracts, and the presence of m^6A alters the local structure of U-rich RNA hairpins, enabling binding of the HNRNPC protein. Numerous instances of these so-called "m^6A switches" were found transcriptome-wide [80]. Another HNRNP member, HNRNPG, binds m^6A-methylated RNAs through its C-terminal low-complexity region, and its depletion disrupts alternative splicing [79]. HNRNPA2B1 has also been characterized as a nuclear reader playing a role in alternative splicing [82]. HNRNPA2B1 was shown to facilitate the processing of select precursor miRNAs into mature miRNAs, but the specific substrate usage of HNRNPC A/B/C has yet to be explored [13,82].

m^6A and embryonic development

m^6A plays a particularly critical role in developmental contexts, as it is thought to be enriched in transcripts controlling cell pluripotency and differentiation [33,65]. Therefore, m^6A has been proposed to help mediate the flow of information from transcription to translation[14]. YTHDF2 mediated decay was shown to be important in embryonic development, playing a role in coordinating transcriptome turnover [14,33]. Ablation of YTHDF2 delayed the clearance of m^6A modified transcripts in zebrafish embryos, thereby compromising the maternal-to-zygotic transition [33]. In mice, absence of YTHDF2 results in defective RNA turnover during oocyte maturation,

leading to female infertility and impaired differentiation of many cell types [65]. Pluripotency factors such as *Nanog* are m^{6}A modified, and thus depletion of either METTL3 or YTHDF2 leads to impaired differentiation, as impaired decay of pluripotency transcripts causes developmental arrest [13].

Roles for m^{6}A readers in post-transcriptional gene regulation during cellular stress

Both heat shock and UV radiation cause increased 5' UTR methylation in mRNAs. In this context, cap-independent translation of stress inducible transcripts occurs[42,43]. Eukaryotic translation initiation factor 3 (eIF3) has been shown to act as a reader when m^{6}A occurs in the 5' UTR, directly recruiting the 40s ribosome and thereby promoting cap-independent translation in the absence of the eIF4F translation initiation complex [43]. Translation can be recapitulated *in vitro* with purified components with the additional of a single m^{6}A to the 5'UTR of an mRNA lacking a 5' cap structure[43]. In addition, the ATP-binding cassette subfamily F member 1 (ABCF1) was characterized as playing a role in m^{6}A-dependent, 5' cap-independent translation. When eIF4F-dependent translation is silenced, m^{6}A in the 5'UTR interacts with eIF3 and ABCF1, which in turn facilitate recruitment of the ternary complex to mediate translation of non-terminal oligopyrimidine (non-TOP) mRNAs [83]. Furthermore, in mouse embryonic fibroblasts and HeLa cells, YTHDF2 relocalizes from the cytoplasm to the nucleus upon heat shock stress, binding to m^{6}A sites in the 5'UTR of transcripts, which in turn may limit demethylation by FTO [42]. This preservation of 5'UTR methylation is proposed to enhance cap-independent translation of heat shock induced transcripts, such as *Hsp70*. Given the dynamic nature of the m^{6}A modification, and the demonstrated role for m^{6}A in facilitating transitions between cell state during development and cellular stress, we wondered whether novel functions for the m^{6}A would also occur during KSHV lytic reactivation.

Overview: RNA modifications in the KSHV lifecycle

While many nuclear replicating viruses have been shown to contain m^{6}A in their mRNA, no studies mapping the global abundance of m^{6}A in viral RNA were published at the time this study was initiated. Thus, we sought to determine the transcriptome-wide profile of m^{6}A during KSHV reactivation. Considering the wide variety of functions attributed to m^{6}A binding proteins, we could only speculate as to how m^{6}A might impact the viral lifecycle. Conceptually, m^{6}A could enhance the export and splicing of viral mRNA through YTHDC1, enhance translation initiation through YTHDF1, or enhance mRNA decay through YTHDF1/2/3. While one of these phenotypes could be dominant, another possibility is that these readers could work in concert to promote "fast-track" processing of modified viral mRNA, leading to increased protein production relative to the half-life of the transcript [14]. Alternatively, if m^{6}A were enriched in immune response transcripts and not in viral transcripts, then possibly faster mRNA processing kinetics could favor production of host anti-viral proteins, thus hindering viral replication. To this end, we sought to address three main aims: 1) To what extent are KSHV mRNAs m^{6}A modified? 2) How does m^{6}A impact KSHV gene expression? 3) Is the impact of m^{6}A cell type specific?

Chapter 2: N^6-methyladenosine modification and the YTHDF2 reader protein play cell type specific roles in lytic viral gene expression during Kaposi's sarcoma-associated herpesvirus infection

This section is adapted from the following publication:
PLoS Pathog. 2018;14: e1006995. doi:10.1371/journal.ppat.1006995
Figures and tables have been renumbered, and the text has been adjusted accordingly. Figure 11 was the only figure generated after publication.

Abstract

Methylation at the N^6 position of adenosine (m^6A) is a highly prevalent and reversible modification within eukaryotic mRNAs that has been linked to many stages of RNA processing and fate. Recent studies suggest that m^6A deposition and proteins involved in the m^6A pathway play a diverse set of roles in either restricting or modulating the lifecycles of select viruses. Here, we report that m^6A levels are significantly increased in cells infected with the oncogenic human DNA virus Kaposi's sarcoma-associated herpesvirus (KSHV). Transcriptome-wide m^6A-sequencing of the KSHV-positive renal carcinoma cell line iSLK.219 during lytic reactivation revealed the presence of m^6A across multiple kinetic classes of viral transcripts, and a concomitant decrease in m^6A levels across much of the host transcriptome. However, we found that depletion of the m^6A machinery had differential pro- and anti-viral impacts on viral gene expression depending on the cell-type analyzed. In iSLK.219 and iSLK.BAC16 cells the pathway functioned in a pro-viral manner, as depletion of the m^6A writer METTL3 and the reader YTHDF2 significantly impaired virion production. In iSLK.219 cells the defect was linked to their roles in the post-transcriptional accumulation of the major viral lytic transactivator ORF50, which is m^6A modified. In contrast, although the ORF50 mRNA was also m^6A modified in KSHV infected B cells, ORF50 protein expression was instead increased upon depletion of METTL3, or, to a lesser extent, YTHDF2. These results highlight that the m^6A pathway is centrally involved in regulating KSHV gene expression, and underscore how the outcome of this dynamically regulated modification can vary significantly between cell types.

Introduction

The addition of chemical modifications is critical to many steps of mRNA processing and the regulation of mRNA fate. There are more than 100 different RNA modifications, but the most abundant internal modification of eukaryotic mRNAs is N^6-methyladenosine (m^6A), which impacts nearly every stage of the posttranscriptional mRNA lifecycle from splicing through translation and decay [10,14,33,61,62,69]. The breadth of impacts ascribed to the m^6A mark can be attributed to its creation of new platforms for protein recognition, in part via local changes to the RNA structure [10,43,79-81,84,85]. The reversibility of m^6A deposition through the activity of demethylases termed erasers adds a further layer of complexity by enabling dynamic regulation, for example during developmental transitions and stress [10,11,14,33,42,86]. Deposition of m^6A occurs co- or post-transcriptionally through a complex of proteins with methyltransferase activity known as writers, which include the catalytic subunit METTL3 and cofactors such as METTL14 and WTAP [10,11,14,35,87]. The modification is then functionally 'interpreted' through the selective binding of m^6A reader proteins, whose interactions with the mRNA promote distinct fates.

The best-characterized m^6A readers are the YTH domain proteins. The nuclear YTHDC1 reader promotes exon inclusion [69], whereupon m^6A-containing mRNA fate is guided in the cytoplasm by the YTHDF1-3 readers. Generally speaking, YTHDF1 directs mRNAs with 3' UTR m^6A modifications to promote translation [62], whereas YTHDF2 recruits the CCR4-NOT deadenylase complex to promote mRNA decay [66]. YTHDF3 has been proposed to serve as a co-factor to potentiate the effects of YTHDF1 and 2 [62-64]. Although the individual effects of YTHDF1 and 2 seem opposing, the

YTHDF proteins may coordinate to promote accelerated mRNA processing during developmental transitions and cellular stress [14]. YTHDC2, the fifth member of the YTH family proteins, was recently shown to play critical roles in mammalian spermatogenesis through regulating translation efficiency of target transcripts [76]. Additional examples of distinct functions for m^6A readers under specific contexts such as heat shock are rapidly emerging [42].

Given the prevalence of the m^6A modification on cellular mRNAs, it is not surprising that a number of viruses have been shown to contain m^6A in their RNA [41,47,48,88-92]. Indeed, a potential viral benefit could be a less robust innate antiviral immune response, as m^6A modification of in vitro synthesized RNAs diminishes recognition by immune sensors such as TLR3 and RIG-I [12,93]. That said, the functional consequences of viral mRNA modification appear diverse and include both pro- and anti-viral roles. In the case of Influenza A, a negative sense ssRNA virus, m^6A and the reader YTHDF2 have been shown to promote viral replication [40]. Furthermore, multiple studies have mapped the sites of m^6A modification in the human immunodeficiency virus (HIV) genome, and shown that it promotes the nuclear export of HIV mRNA as well as viral protein synthesis and RNA replication [88,89,91]. Roles for the YTHDF proteins in during HIV infection remain varied however, as Tirumuru and colleagues propose they function in an anti-viral context by binding viral RNA and inhibiting reverse transcription, while Kennedy and colleagues observe they enhance HIV replication and viral titers [88,91]. A more consistently anti-viral role for the m^6A pathway has been described for the *Flaviviridae*, whose (+) RNA genomes are replicated exclusively in the cytoplasm and contain multiple m^6A sites in their genomic RNA [41,47]. An elegant study by Horner and colleagues showed that depletion of m^6A writers and readers or the introduction of m^6A-abrogating mutations in the viral E1 gene all selectively inhibit hepatitis C virus (HCV) assembly [41]. Similarly, depletion of METTL3 or METTL14 enhances Zika virion production [47].

Despite the fact that m^6A modification of DNA viruses was first reported more than 40 years ago for simian virus 40, herpes simplex virus type 1, and adenovirus type 2, roles for the modification in these and other DNA viruses remain largely unexplored [94-98]. Unlike most RNA viruses, with few exceptions DNA viruses replicate in the nucleus and rely on the cellular transcription and RNA processing machinery, indicating their gene expression strategies are likely interwoven with the m^6A pathway. Indeed, it was recently shown that the nuclear reader YTHDC1 potentiates viral mRNA splicing during lytic infection with Kaposi's sarcoma-associated herpesvirus (KSHV) [71]. Furthermore, new evidence suggests m^6A modification potentiates the translation of late SV40 mRNAs [99] , further indicating that this pathway is likely to exert a wide range of effects on viral lifecycles.

Here, we sought to address roles for the m^6A pathway during lytic KSHV infection by measuring and mapping the abundance of m^6A marks across the viral and host transcriptome. This gammaherpesvirus remains the leading etiologic agent of cancer in AIDS patients, in addition to causing the lymphoproliferative disorders multicentric Castleman's disease and primary effusion lymphoma. The default state for KSHV in cultured cells is latency, although in select cell types the virus can be reactivated to engage in lytic replication, which involves a temporally ordered cascade of gene expression. We reveal that m^6A levels are significantly increased upon KSHV

reactivation, which is due to a combination of m^{6}A deposition across multiple kinetic classes of viral transcripts and a concomitant decrease in m^{6}A levels across much of the host transcriptome. Depletion of m^{6}A writer and cytoplasmic reader proteins impaired viral lytic cycle progression in the KSHV iSLK.219 and iSLK.BAC16 reactivation models, suggesting this pathway potentiates the KSHV lytic cycle. Interestingly, however, the roles for the m^{6}A writer and readers shifted to instead display neutral or anti-viral activity in the TREX-BCBL-1 reactivation model. These findings thus demonstrate that while KSHV mRNAs are marked by m^{6}A, the functional consequences of this mark can vary significantly depending on cell context, reinforcing both the functional complexity and dynamic influence of m^{6}A.

Results

KSHV mRNA contains m^{6}A modifications

Epitranscriptome mapping has revealed significant roles for the m^{6}A pathway in the lifecycle and regulation of several RNA viruses, but at the time we initiated these studies, similar global analyses had yet to be performed for a DNA virus. Given that herpesviral mRNAs are transcribed and processed in the nucleus using the cellular RNA biogenesis machinery, we hypothesized that these viruses would engage the m^{6}A pathway. We therefore first quantified how KSHV reactivation impacted total cellular m^{6}A levels in the KSHV-positive renal carcinoma cell line iSLK.219 (**Fig 1**). These cells are a widely used model for studying viral lytic events, as they stably express the KSHV genome in a tightly latent state but harbor a doxycycline (dox)-inducible version of the major viral lytic transactivator ORF50 (also known as RTA) that enables efficient entry into the lytic cycle [100,101]. Polyadenylated (polyA+) RNA was enriched from untreated (latent) or dox-reactivated iSLK.219 cells and the levels of m^{6}A were quantitatively analyzed by liquid chromatography-tandem mass spectrometry (LC-MS/MS) (**Fig 1A**). Indeed, we observed a three-fold increase in total m^{6}A levels upon KSHV lytic reactivation, suggesting that m^{6}A deposition significantly increased during viral replication (**Fig 1B**).

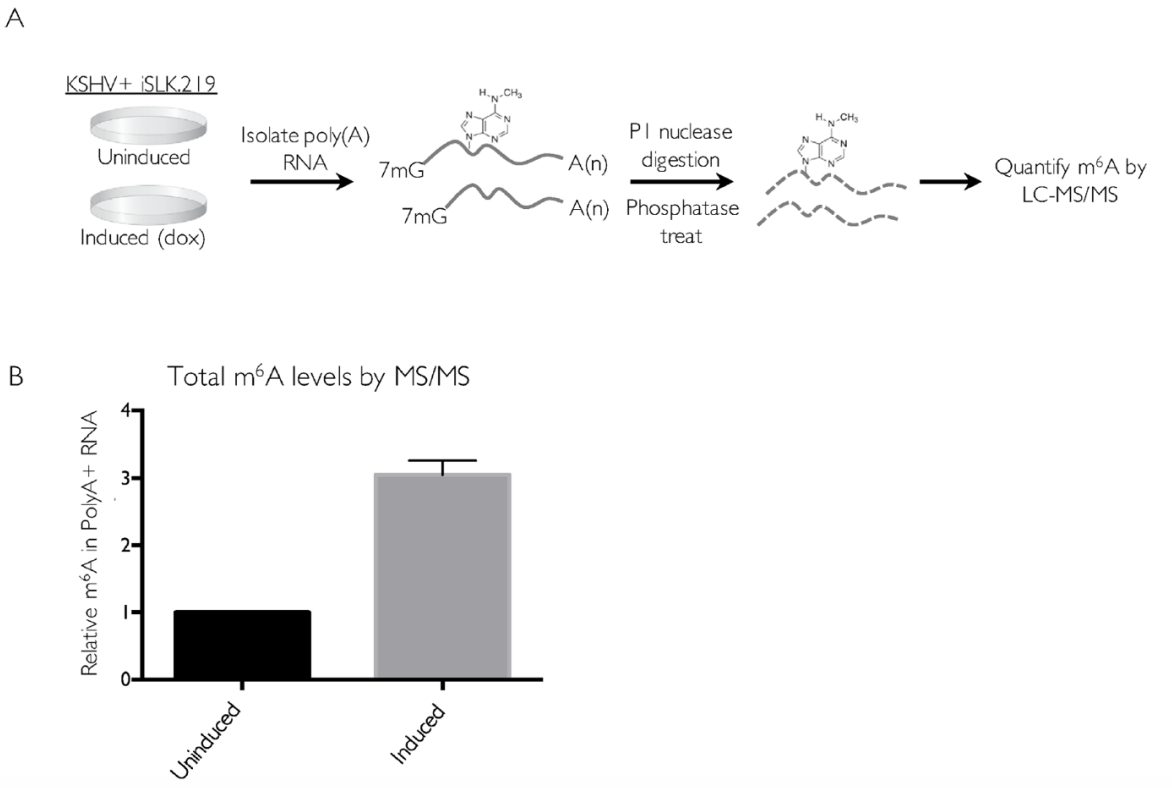

Fig 1. m^{6}A increases upon KSHV reactivation. (A) Schematic of the experimental setup. iSLK.219 cells were induced with doxycycline for 5 days to induce the lytic cycle, and total RNA was collected and subjected to oligo dT selection to purify poly(A) RNA. Polyadenylated RNA was spiked with 10 μM of 5-fluorouridine and digested with nuclease P1 and alkaline phosphatase, and subjected to LC-MS/MS analysis. (B) Relative m^{6}A content in iSLK.219 cells. The induced sample was normalized with respect to the uninduced sample (set to 1).

We next sought to discern whether the increase in m^{6}A during the KSHV lytic cycle favors host or viral mRNAs using high throughput m^{6}A RNA sequencing (m^{6}A-seq) [16]. This technique can reveal both the relative abundance and general location of m^{6}A in KSHV and cellular mRNA. Total m^{6}A containing RNA was immunoprecipitated from 2 biological replicates of latent or lytically reactivated iSLK.219 cells using an m^{6}A-specific antibody. DNase-treated total mRNA was fragmented to lengths of 100 nt prior to immunoprecipitation and then subjected to m^{6}A-seq. Total RNA-seq was run in parallel for each sample, allowing the degree of m^{6}A modification to be normalized with respect to transcript abundance because the levels of many transcripts change upon viral lytic reactivation. Peaks with a fold-change four or higher (FC>4) and a false discovery rate of 5% or lower (FDR>5%) in both replicates were considered significant, although it is possible that additional transcripts detectably modified to lower levels or in a more dynamic manner may also be functionally regulated by m^{6}A (complete list of viral peaks with FC>2 in **Tables 1.1-1.4**). In lytically reactivated samples, 10 transcripts comprising genes of immediate early, early, and late kinetic classes displayed significant m^{6}A modification in both replicates (**Fig 2A** and **Fig 3**). Within these KSHV mRNAs, m^{6}A peaks were detected primarily in coding regions, although in some cases the location of a peak in a coding region overlaps with a UTR (**Fig 3)**. Furthermore, all but one peak contains at least one instance of the GG(m^{6}A)C consensus sequence.

While many of the modified viral transcripts contained only one m^6A peak, multiple peaks were found in certain transcripts, including the major lytic transactivator ORF50 (**Fig 2B**). Of note, exon2 of ORF50 contained one m^6A peak of FC>4 in replicate one, and three m^6A peaks in replicate two, each of which have at least one m^6A consensus motif, further increasing confidence that these peaks accurately represent m^6A modified sites. Furthermore, the viral ncRNA PAN, which has been reported to comprise over 80% of nuclear PolyA+ RNA during lytic reactivation [102], contains FC>4 peaks in both replicates. Modification of PAN likely accounts for the marked three-fold increase in cellular m^6A content observed upon lytic reactivation (**Fig 1B**). As anticipated given the restricted viral gene expression profile during latency, unreactivated samples had many fewer m^6A containing viral mRNAs, with the only FC>4 peaks occurring in both replicates located in ORF4. Although ORF4 is a lytic transcript, its coding region overlaps with the 3' UTR of K1, which is expressed during both the latent and lytic phases of the viral lifecycle (**Fig 2A**, **Fig 3**) [103,104].

To validate the m^6A-seq results, we performed m^6A RNA immunoprecipitation (RIP) followed by quantitative real-time PCR (RT-qPCR) on six of the viral transcripts predicted to be m^6A modified from the m^6A-seq data. This technique allows determination of the relative level of m^6A content in a given transcript compared to an unmodified transcript. As controls, we included primers for the cellular GAPDH transcript, which is known not to be m^6A modified, and the Dicer transcript, which is m^6A modified [16]. The m^6A RIP RT-qPCR confirmed modification of the vIL-6, K1, ORF50, ORF57 and PAN viral transcripts, in agreement with m^6A-seq results (**Fig 2C**). In summary, we found m^6A modification in approximately one third of KSHV transcripts upon lytic reactivation, consistent with the hypothesis that this pathway contributes to KSHV gene expression.

We next compared the distribution of m^6A peaks in host mRNAs from unreactivated versus reactivated cells to assess whether lytic KSHV infection altered the m^6A profile of cellular transcripts. Analyzing the two independent replicates for each condition, we found an average of 14,092 m^6A modification sites (FC>4 and FDR>5%) in host transcripts pre-reactivation, compared to 10,537 peaks post-reactivation (**Fig 2D**). We observed that this >25% decrease in m^6A deposition on cellular mRNA encompassed a wide spectrum of transcripts, and no notable patterns were apparent by GO term analysis for functional categories enriched in the altered population. Thus, while the functional impact of the altered host m^6A profile remains unresolved, the observation that KSHV lytic infection increased the level of m^6A in total poly A+ RNA despite decreasing its presence in cellular mRNA implies that m^6A deposition during infection favors viral transcripts.

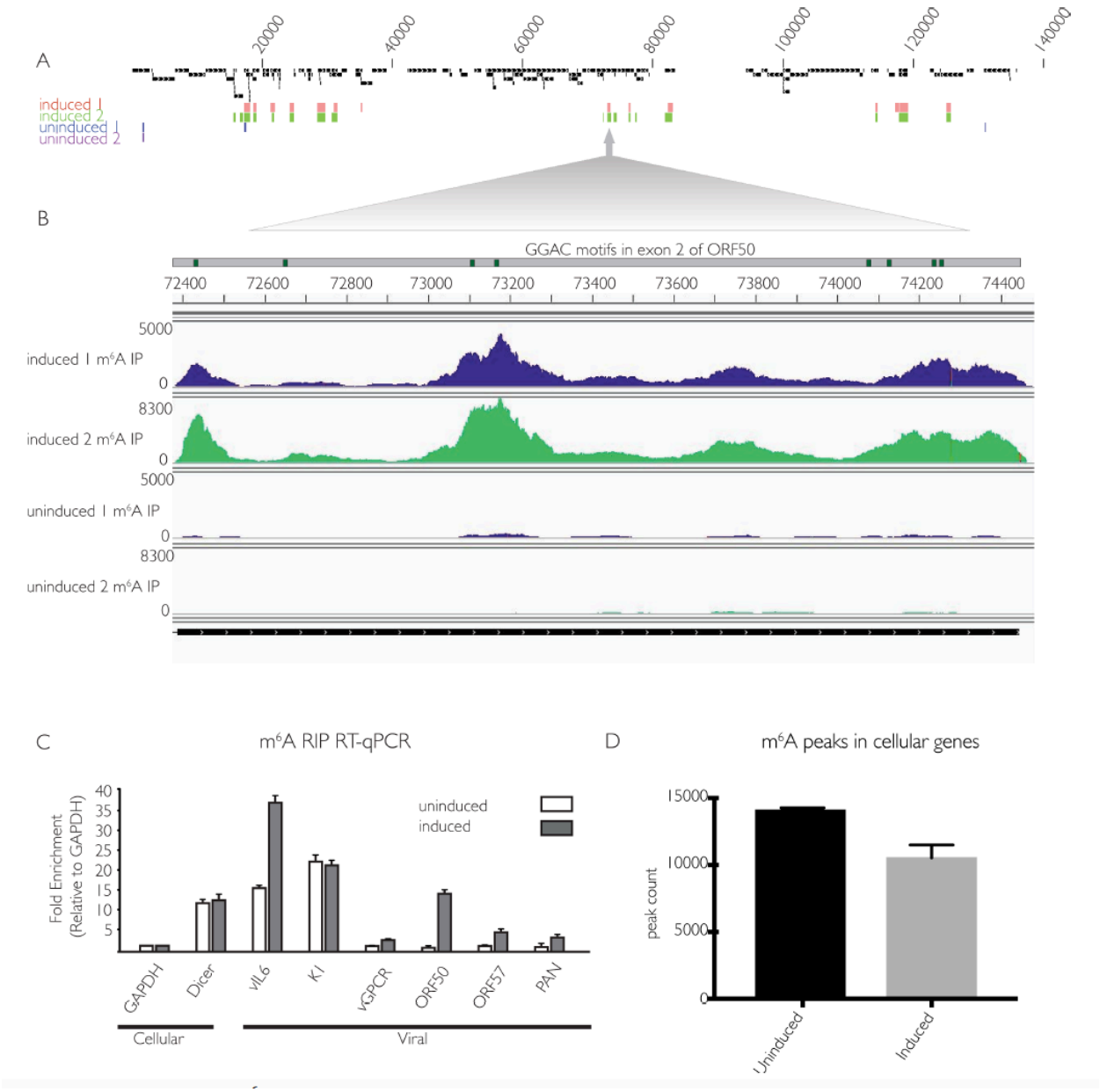

Fig 2. KSHV mRNA contains m^{6}A modifications. (A) Two independent replicates of iSLK.219 cells containing latent KSHV were treated with dox for 5 days to induce the viral lytic cycle (induced) or left untreated to preserve viral latency (uninduced). DNase-treated RNA was isolated and subjected to m^{6}Aseq. Displayed are peaks with a fold change of four or higher, comparing reads in the m^{6}A-IP to the corresponding input. Numbers above peaks correspond to the base position within the KSHV genome. (B) Overview of sequencing reads from induced and uninduced m^{6}A IP samples, aligned to the ORF50 transcript and the annotated GG(m^{6}A)C consensus motifs found in exon 2 of ORF50. Numbers to the left of sequencing reads indicate the scale of the read count. (C) Cells were induced as in (A), and total RNA was subjected to m^{6}A RIP, followed by RT-qPCR using primers for the indicated viral and cellular genes. Values are displayed as fold change over input, normalized to GAPDH. (D) Quantification of cellular m^{6}A peaks from m^{6}Aseq analysis.

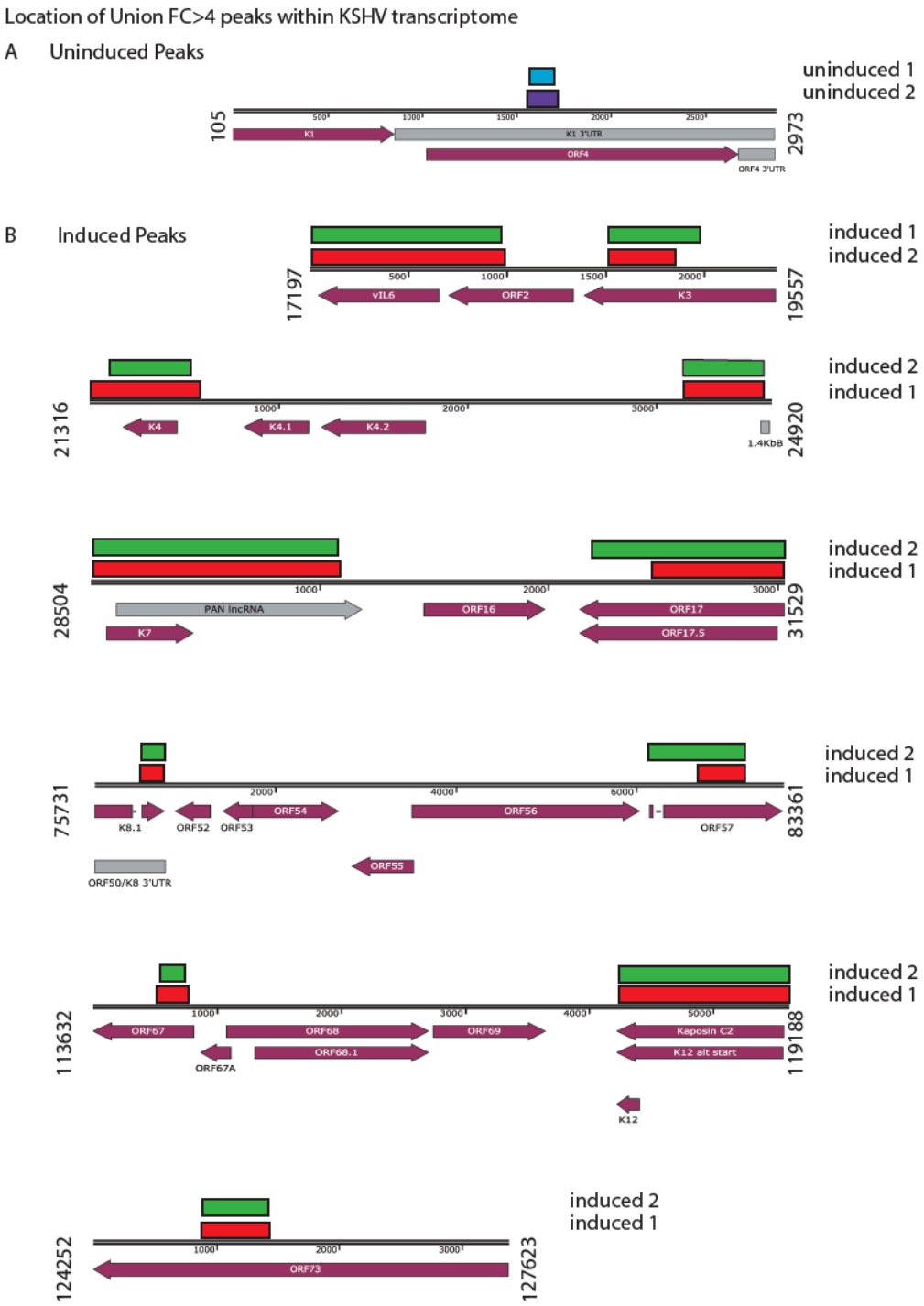

Fig 3. Location of union FC>4 peaks within KSHV transcriptome. Overview of sequencing reads aligned to regions of the KSHV transcriptome containing m^6A modifications. Depicted are peaks with a fold change of four or higher in both replicates, comparing reads in the m^6A-IP to the corresponding input. The blue and purple bars denote the sequences encompassed by the FC>4 peaks in each uninduced replicate (A), while the red and green colored bars denote the FC>4 peaks in each induced replicate (B). In the reference transcriptome, grey bars indicate annotated 3'UTRs or ncRNAs, while burgundy arrows depict ORFs. Note that the alignment of the ORF50 induced peaks can be found in Figure 2.

m^{6}A and the reader YTHDF2 mediate viral gene expression and virion production in iSLK.219 cells

Given the significant deposition of m^{6}A across KSHV transcripts, we reasoned that m^{6}A might play an important role in potentiating the viral lifecycle. We therefore examined the effect of depleting the m^{6}A writers and readers on KSHV virion production using a supernatant transfer assay. The KSHV genome in iSLK.219 cells contains a constitutively expressed version of GFP, which allows for fluorescence-based monitoring of infection by progeny virions. We performed siRNA-mediated knockdown of METTL3, the catalytic subunit responsible for m^{6}A deposition, as well as the m^{6}A readers YTHDF 1, 2 and 3 (**Fig 4A**). Cells were then treated with dox and sodium butyrate to induce lytic reactivation for 72 hr, whereupon supernatants were collected and used to infect 293T recipient cells. The number of GFP positive 293T cells at 24 hpi was measured by flow cytometry (**Fig 4B**). Notably, for virus generated from METTL3 depleted cells, only 7% of recipient cells were infected compared to 82% for virus generated during treatment with a control siRNA (**Fig 4B**). YTHDF2 depletion caused an even more pronounced defect, resulting in a near absence of virion production (**Fig 4B**). In contrast, YTHDF3 knockdown resulted in only modest changes in virion production, while virion production was unaffected by YTHDF1 knockdown (**Fig 4B**). The prominent defect in virion production in METTL3 and YTHDF2 depleted cells was not due to knockdown-associated toxicity, as we did not observe changes in cell viability in siRNA treated cells (representative experiment shown in **Fig 5**). Furthermore, we validated the results for YTHDF2 and YTHDF3 using independent siRNAs (**Fig 5**). Thus, the m^{6}A writer METTL3 and the reader YTHDF2 play important roles in driving KSHV infectious virion production in iSLK.219 cells.

We then sought to determine the stage of the viral lifecycle impacted by the m^{6}A pathway by measuring the impact of writer and reader depletion on the abundance of viral mRNAs of different kinetic classes. First, levels of representative immediate early, delayed early, and late viral mRNAs were measured by RT-qPCR following lytic reactivation for 72 hr. ORF50 and K8.1 transcripts contained at least one m^{6}A peak, while ORF37 did not appear to be significantly modified in our m^{6}A-seq data (see **Table 1.1-1.4**). METTL3 depletion did not appear to impact accumulation of the ORF50 immediate early or ORF37 delayed early mRNAs at this time point, but resulted in a significant defect in accumulation of the K8.1 late gene mRNA (**Fig 4C**). Consistent with the virion production data, we observed a striking and consistent defect in the accumulation of each of the viral transcripts upon YTHDF2 depletion, suggesting that this protein is essential for lytic KSHV gene expression beginning at the immediate early stage (**Fig 4C**). Similar results were observed using an independent YTHDF2-targeting siRNA (**Fig 5**)**.** We also observed a prominent defect in accumulation of ORF50 and the delayed early ORF59 proteins by Western blot specifically upon YTHDF2 depletion (**Fig 4D**). In contrast, depletion of YTHDF1 or YTHDF3 did not reproducibly impact ORF50, ORF37, or K8.1 gene expression at 72 hr post reactivation (**Fig 4C**).

In agreement with the above findings, we also observed that iSLK.219 cells depleted of METTL3 and YTHDF2 displayed a prominent defect in viral reactivation, as measured by expression of red fluorescent protein (RFP) driven by the PAN lytic cycle promoter from the viral genome (**Fig 4E**). Similarly, ORF50 protein production was also markedly

reduced upon METTL3 or YTHDF2 depletion at the 24 hr time point, which represents the early phase of the lytic cycle (**Fig 4F**).

To determine whether the effects of the m^6A pathway on ORF50 were dependent on KSHV infection, we measured ORF50 protein in an uninfected iSLK cell line containing only the integrated, dox-inducible ORF50 gene (iSLK.puro cells) (**Fig 4G**). Similar to our findings with infected iSLK.219 cells, depletion of METTL3 or YTHDF2 strongly reduced ORF50 protein levels (**Fig 4H**). YTHDF3 depletion resulted in an increase in ORF50 expression, which we also observed to a more modest degree in the iSLK.219 cells (see **Fig 4D**). Collectively, these results suggest that m^6A modification is integral to the KSHV lifecycle, and that YTHDF2 plays a particularly prominent role in mediating KSHV lytic gene expression in iSLK.219 cells. They further indicate that m^6A modification can impact ORF50 expression in both uninfected and KSHV infected iSLK cells.

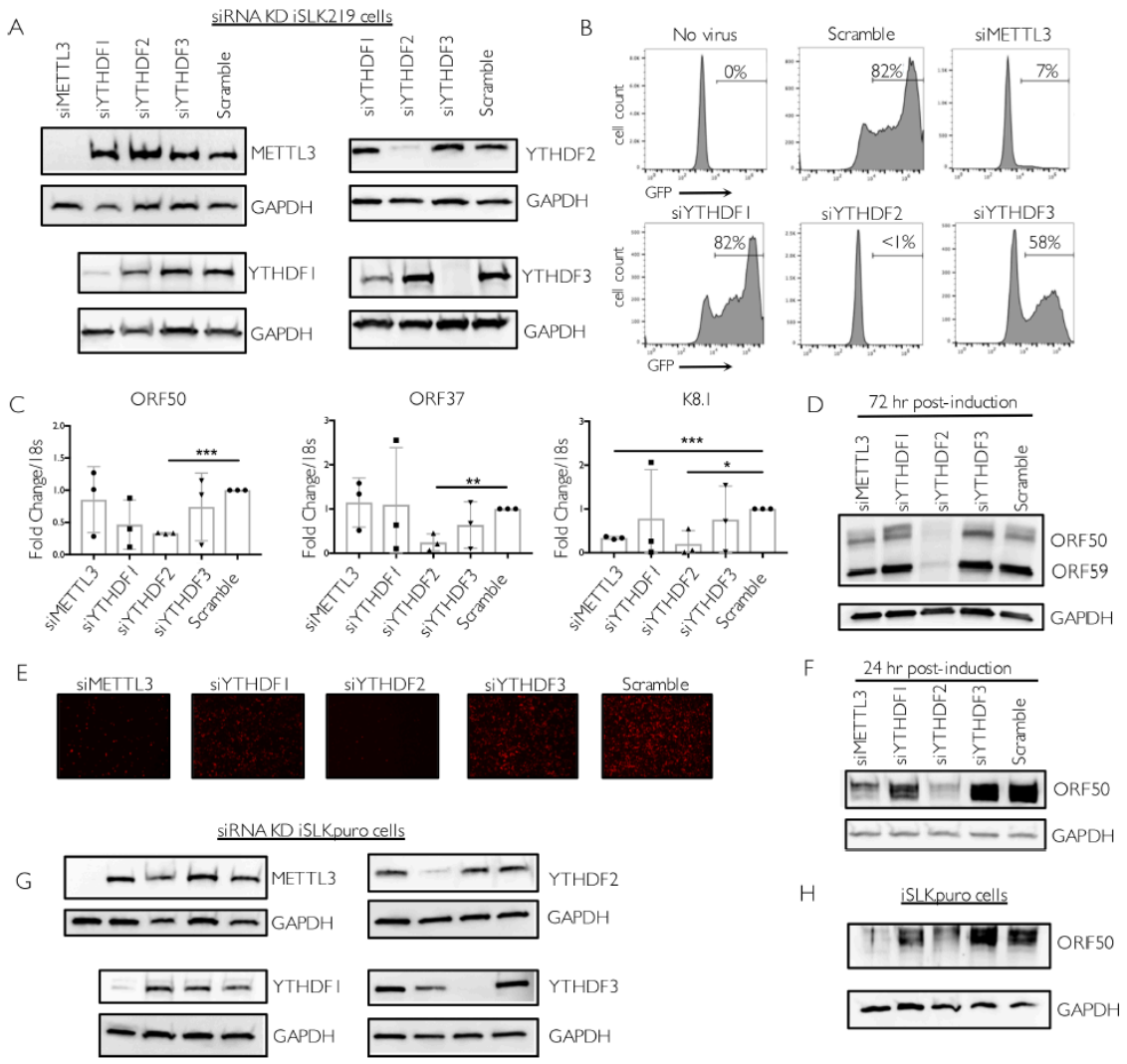

Fig 4. m^{6}A and the reader YTHDF2 potentiate viral gene expression and virion production in iSLK.219 cells. Cells were transfected with control scramble (scr) siRNAs or siRNAs against METTL3, YTHDF1, 2, or 3, then reactivated for 72 hr with doxycycline and sodium butyrate. (A) Knockdown efficiency was measured by western blot using antibodies for the indicated protein, with GAPDH serving as a loading control in this and all subsequent figures. (B) Viral supernatant was collected from the reactivated iSLK.219 cells and transferred to uninfected HEK293T recipient cells. 24 hr later, the recipient cells were analyzed by flow cytometry for the presence of GFP, indicating transfer of infectious virions. (C) ORF50, ORF37 and K8.1 gene expression was analyzed by RT-qPCR from cells treated with the indicated siRNAs. Data are from 3 independent experiments. Unpaired Student's t test was used to evaluate the statistical difference between samples. Significance is shown for P values <0.05 (*), $\leq$ 0.01 (**), and $\leq$ 0.001 (***). (D) Expression of the viral ORF50 and ORF59 proteins in cells treated with the indicated siRNAs was measured by western blot 72 hr post-reactivation. (E) Unreactivated iSLK.219 cells containing latent virus were treated with control scramble (scr) siRNAs or siRNAs targeting METTL3, YTHDF1, YTHDF2, or YTHDF3. The cells were then reactivated with dox and sodium butyrate for 48 hr and lytic reactivation was monitored by expression of the lytic promoter-driven red fluorescent protein. (F) Protein was harvested from the above described cells and subjected to western blot for ORF50 and the control GAPDH protein at 24 hr post-reactivation. (G-H) Uninfected iSLK.puro cells expressing DOX-inducible RTA were transfected with the indicated siRNAs for 48 hr, then treated with dox for 24 hr to induce ORF50 expression. Knockdown efficiency *(G)* and ORF50 protein levels *(H)* were measured by western blot using antibodies for the indicated protein, with GAPDH serving as a loading control.

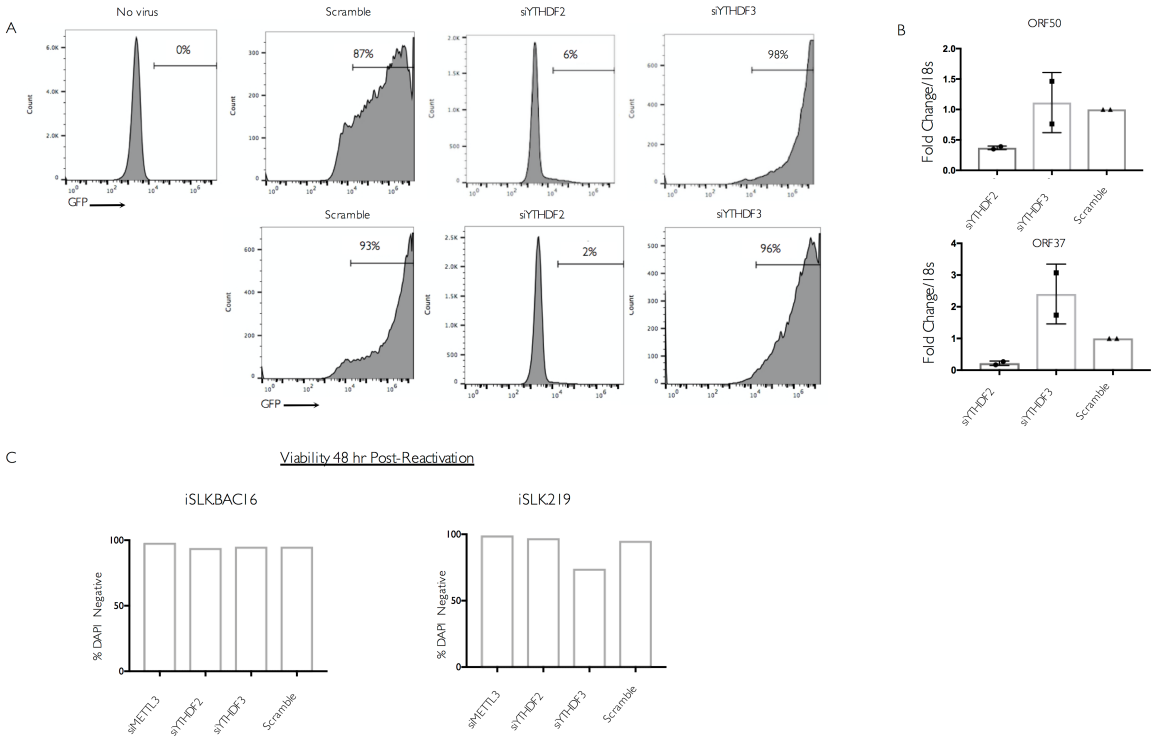

Fig 5. Confirmation of Fig 4 results using independent siRNAs (A) Independent siRNAs against YTHDF2 and YTHDF3 yield similar results as those shown in Fig 4. Cells were transfected with control scramble (scr) siRNAs (Qiagen SI03650318) or siRNAs against YTHDF2 (Qiagen SI04174534) or YTHDF3 (Qiagen SI00764778), then reactivated for 72 hr with doxycycline and sodium butyrate. Viral supernatant was collected from the reactivated iSLK.219 cells and transferred to uninfected HEK293T recipient cells. 24 hr later, the recipient cells were analyzed by flow cytometry for the presence of GFP, indicating transfer of infectious virions. Data are from 2 independent experiments, with each replicate shown. (B) ORF50 and ORF37 gene expression was analyzed by RT-qPCR from the above cells at the time of supernatant transfer. (C) Viability of iSLK.BAC16 and iSLK.219 cells following siRNA transfection. Cells were transfected with the indicated siRNAs for 48 hr, followed by lytic reactivation with dox and sodium butyrate for 48 hr. Cells were collected and diluted 1:1 with Trypan blue prior to counting on a Countess II Automated Cell Counter. One representative experiment is shown.

The m^{6}A pathway post-transcriptionally controls ORF50 expression in iSLK.219 cells, leading to a subsequent defect in transcriptional feedback at the ORF50 promoter.

ORF50 is the major viral transcriptional transactivator, and its expression is essential to drive the KSHV lytic gene expression cascade [105]. The observations that ORF50 is m^{6}A modified and that its accumulation is dependent on YTHDF2 indicate that the m^{6}A pathway plays key roles in ORF50 mRNA biogenesis or fate in iSLK.219 cells, potentially explaining the lytic cycle progression defect in the knockdown cells. Deposition of m^{6}A has been reported to occur both co-transcriptionally and post-transcriptionally [14,35,87,106] . To determine whether the m^{6}A pathway is important for ORF50 synthesis or its posttranscriptional fate, we measured ORF50 transcription in reactivated iSLK.219 cells upon depletion of METTL3, YTHDF2, or YTHDF3 using 4-thiouridine (4sU) metabolic pulse labeling. 4sU is a uridine derivative that is incorporated into RNA during its transcription, and thiol-specific biotinylation of the 4sU-containing RNA enables its purification over streptavidin-coated beads [107,108]. At 24

hr post reactivation, RNA in the siRNA treated iSLK.219 cells was pulse labeled with 4sU for 30 min, whereupon the labeled RNA was isolated by biotin-streptavidin purification and viral transcripts were quantified by RT-qPCR (**Fig 6A)**. Despite the defect in ORF50 accumulation observed upon YTHDF2 depletion (see **Fig 4F**), we observed no decrease in 4sU-labeled ORF50 mRNA upon depletion of any of the m^6A writer or reader proteins (**Fig 6B**). However, in YTHDF2 depleted cells, there was a prominent defect in the level of 4sU-labeled ORF37, likely because its transcription is dependent on the presence of ORF50 protein (**Fig 6C**).

The ORF50 mRNA detected in the above experiments represents a combination of the mRNA transcribed from the dox-inducible cassette as well as from the KSHV genome [101]. While the dox-inducible promoter is constitutively active under dox treatment, ORF50 transcription from KSHV is sensitive to ORF50 protein levels because it transactivates its own promoter [8]. The decreased ORF50 protein levels observed in Fig 4 might therefore lead to a selective reduction in transcription from the native ORF50 promoter by interfering with this positive transcriptional feedback. Indeed, primers designed to specifically recognize ORF50 derived from the viral genome revealed a marked defect in transcription of KSHV-derived ORF50 upon YTHDF2 depletion, as well as a slight reduction upon METTL3 depletion (**Fig 6D**). Collectively, the above results suggest that m^6A initially functions to post-transcriptionally regulate ORF50 mRNA abundance, but that when ORF50 protein levels fall upon YTHDF2 or METTL3 knockdown, the positive transcriptional feedback mechanism at the viral promoter also becomes restricted.

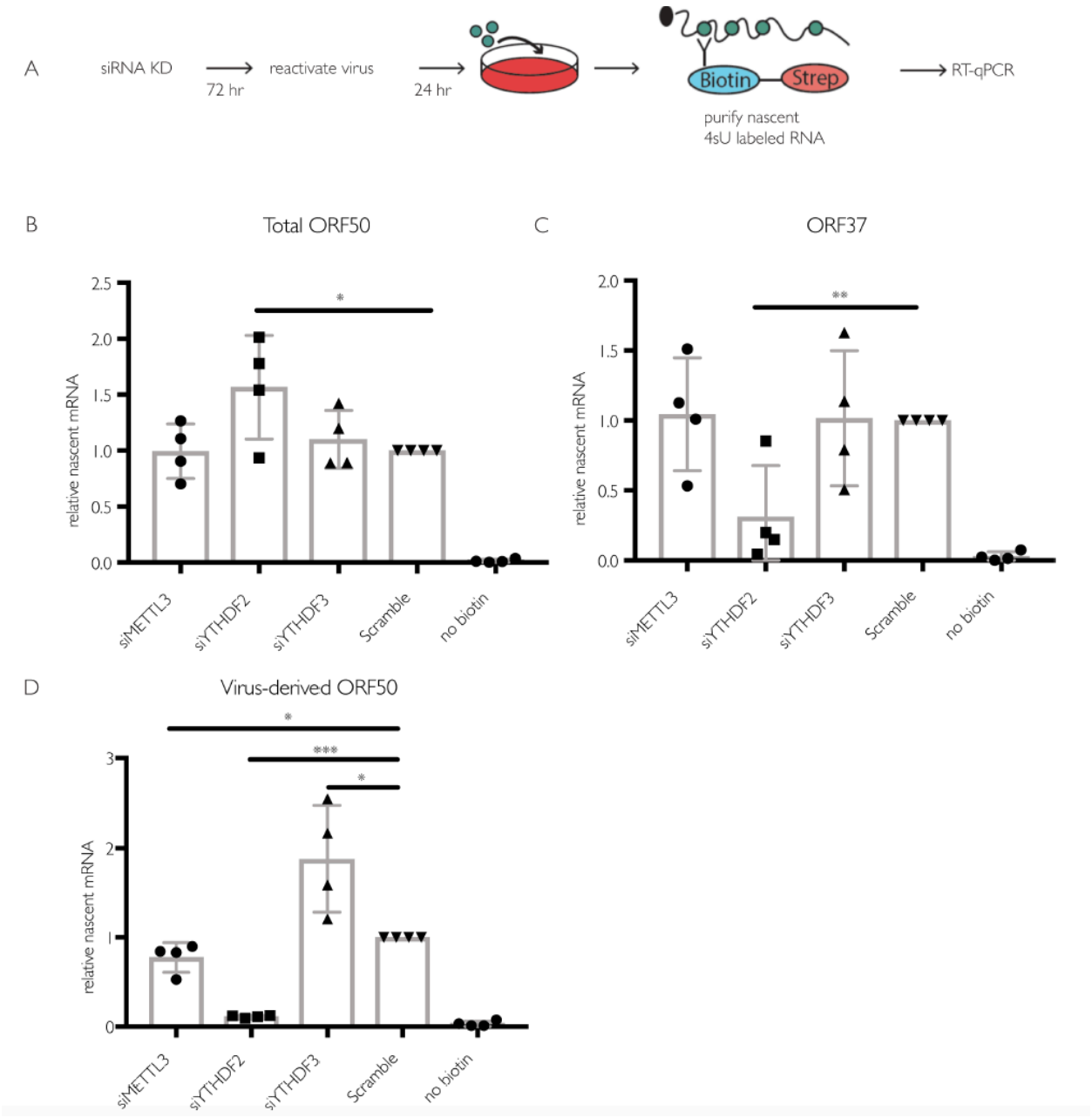

Fig 6. Depletion of the m^{6}A writer and readers does not impact ORF50 nascent transcription in iSLK.219 cells. (A) Schematic of the experimental setup for measuring nascent RNA synthesis. Cells were transfected with the indicated siRNAs for 48 hr then reactivated for 24 hr with dox. 4sU was added for 30 minutes, whereupon 4sU-labeled RNA was isolated using biotin/streptavidin affinity purification, reverse transcribed, and analyzed by RT-qPCR using primers specific to ORF50 or ORF37. (B-D) Levels of 4sU-labeled total ORF50 *(B)*, ORF37 *(C)*, and ORF50 transcribed from the viral genome (virus-derived) (*D*) determined as described above. Unpaired Student's t test was used to evaluate the statistical difference between samples. Significance is shown for P values <0.05 (*), ≤ 0.01 (**), and ≤ 0.001 (***).

The impact of m^{6}A on KSHV infection is cell type specific

To independently validate the METTL3 and YTHDF2 phenotypes, we also evaluated their importance in the iSLK.BAC16 model. Although independently

generated, this is the same cell background as iSLK.219, including the dox-inducible ORF50, but instead contains the viral genome in the context of a bacterial artificial chromosome (BAC16) [109] . Similar to our results with the infected iSLK.219 cells, depletion of METTL3 or YTHDF2 in iSLK.BAC16 cells led to a significant defect in virion production as measured by supernatant transfer assays (**Fig 8A-C**). In addition, the total levels of ORF50 mRNA (from the dox-induced plus viral promoters) were unchanged between the different siRNA treated cells, while depletion of YTHDF2 led to a significant reduction in the level of BAC16-derived ORF50 and K8.1 mRNAs (**Fig 8D**). In contrast, METTL3 depletion did not significantly impact the level of ORF50, ORF37, or K8.1 transcripts. It should be noted that levels of METTL3 knockdown in excess of 80% have only been reported to reduce m^6A levels in Poly A RNA by 20-30% [35]. Thus, at least some fraction of ORF50 (and other) transcripts may still be m^6A modified due to residual enzyme activity of the remaining METTL3. In agreement with these observations, knockdown of METTL3 modestly reduced but did not eliminate the pool of m^6A modified ORF50 or the cellular SON mRNAs in iSLK.BAC16 cells as measured by m^6A RIP RT-qPCR (**Fig 7**). Finally, we observed that although ORF59 protein levels were consistently reduced upon YTHDF2 knockdown, and to a more variable extent upon METTL3 depletion, we did not detect the same marked effects on ORF50 protein levels in iSLK.BAC16 cells as in iSLK.219 cells (**Fig 8E**). In summary, although iSLK.219 and iSLK.BAC16 cells exhibit a somewhat different gene expression profile in the context of YTHDF2 and METTL3 knockdown, depletion of these m^6A pathway components restricts the KSHV lytic lifecycle in both models.

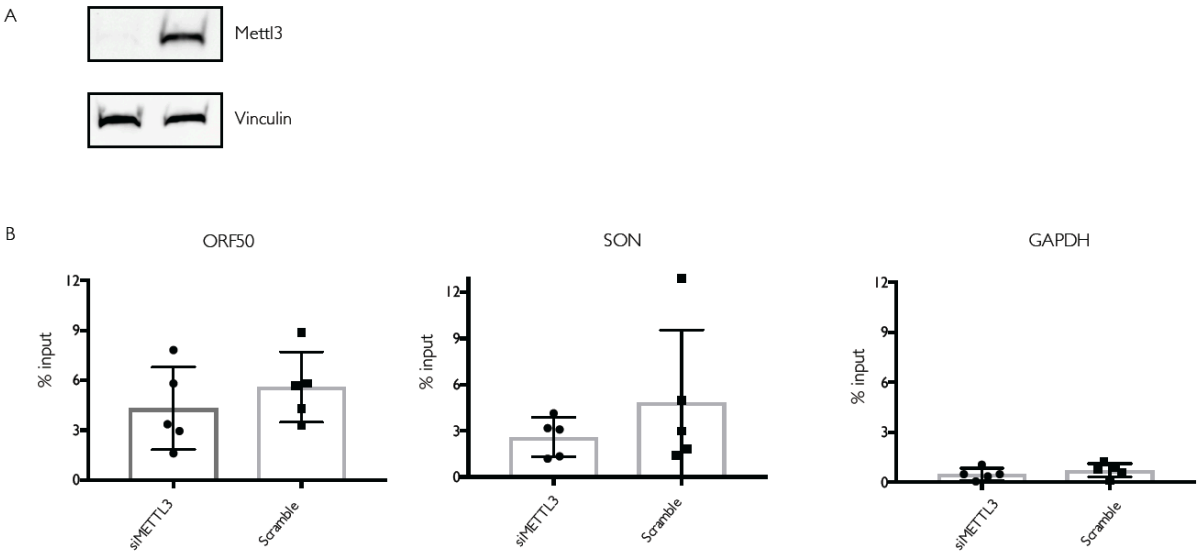

Fig 7. Impact of METTL3 depletion on isolation of m^6A modified mRNA in iSLK.BAC16 cells
iSLK.BAC16 cells were subject to siRNA knockdown using METTL3 or control siRNA for 48 hr. Cells were reactivated for 24 hr with dox. (A) Western blot for knockdown efficiency at time of harvest. (B) Total RNA from harvested cells was then subject to m^6A RIP RT-qPCR for the viral transcript ORF50 and cellular transcripts SON (m^6A modified) and GAPDH (unmodified). Data shown are from 5 independent experimental replicates.

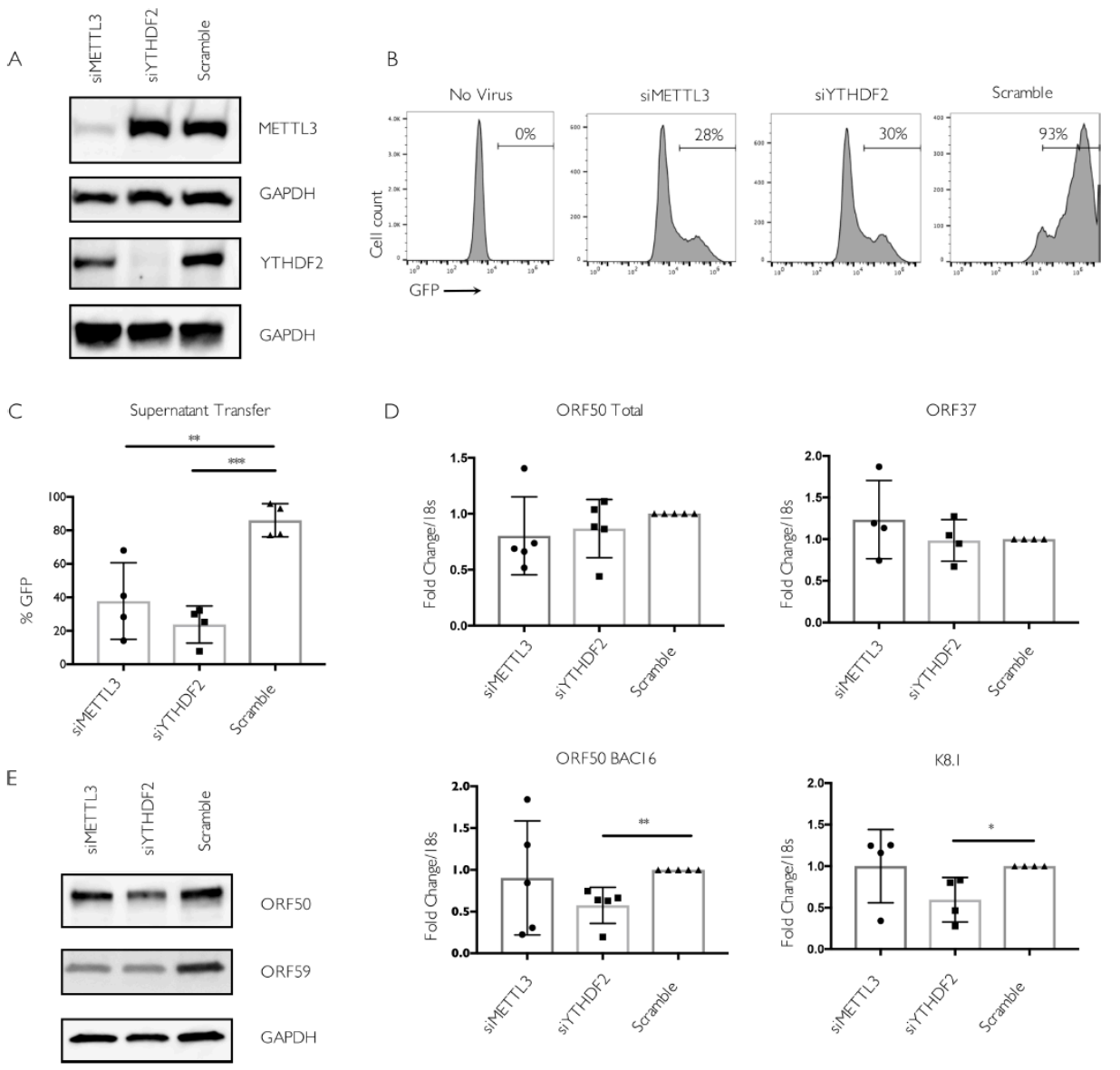

Fig 8. METTL3 and YTHDF2 are important for KSHV lytic replication in iSLK.BAC16 cells. Cells were transfected with control scramble (scr) siRNAs or siRNAs against METTL3 or YTHDF2, then reactivated for 24 hr with doxycycline and sodium butyrate. (A) Knockdown efficiency was measured by western blot using antibodies for the indicated protein. (B) Viral supernatant was collected from the reactivated iSLK.BAC16 cells 72 hr post-reactivation and transferred to uninfected HEK293T recipient cells. 24 hr later, the recipient cells were analyzed by flow cytometry for the presence of GFP, indicating transfer of infectious virions. (C) Quantification of supernatant transfer results from four independent experiments. (D) ORF50, ORF37, and K8.1 gene expression 24 hr post-reactivation was analyzed by RT-qPCR from cells treated with the indicated siRNAs. Data for ORF50 are from five independent experiments, while ORF37 and K8.1 data are from four independent experiments. Unpaired Student's t test was used to evaluate the statistical difference between samples in panels *C-D*. Significance is shown for P values $\leq$ 0.01 (**) and $\leq$ 0.001 (***). (E) Western blots showing expression of the viral ORF50 and ORF59 proteins at 24 hr post reactivation of iSLK.BAC16 cells treated with the indicated siRNAs.

Given the diversity of functions reported for m^6A in controlling cellular processes and virus infections [14,48,90], we also sought to evaluate the role of this pathway in

mediating ORF50 expression in another widely used KSHV infected cell line of distinct origin, the B cell line TREX-BCBL-1 [110]. Similar to iSLK.219 and iSLK.BAC16 cells, TREX-BCBL-1 cells also contain a dox-inducible copy of ORF50 to boost reactivation. First, we evaluated whether the ORF50 transcript was m^6A modified in TREX-BCBL-1 cells by m^6A RIP, followed by RT-qPCR using control or ORF50 specific primers. Indeed, there was a clear enrichment of ORF50 in the reactivated, m^6A-containing RNA population (**Fig 12A**). As expected, we detected the m^6A modified DICER transcript in both reactivated and unreactivated cells, whereas the unmodified GAPDH transcript was present in neither sample (**Fig 12A**). The m^6A pathway components were then depleted from TREX-BCBL-1 cells via siRNA treatment, whereupon cells were reactivated for 72 hr with dox, TPA, and ionomycin. As knockdown efficiency for YTHDF1 was inconsistent in this cell type, we focused on the impact of METTL3, YTHDF2, and YTHDF3. We observed no significant changes in the level of ORF50 mRNA upon METTL3 or YTHDF3 depletion (**Fig 12B, D**). Although there was a consistent decrease in ORF50 mRNA in the YTHDF2 depleted cells, this may be due to the fact that YTHDF2 knockdown modestly decreased the viability of TREX-BCBL1 cells (**Fig 9**). Surprisingly, however, METTL3 knockdown and, to a more variable extent YTHDF2 knockdown, resulted in increased ORF50 protein expression (**Fig 12C,** additional replicate experiments showing ORF50 levels in **Fig 9**). YTHDF3 depletion did not significantly impact ORF50 or ORF59 protein (**Fig 12C**). Thus, unlike in iSLK cells, METTL3 and YTHDF2 appear to restrict ORF50 expression in TREX-BCBL1 cells. These phenotypic differences were not due to distinct virus-induced alterations in the abundance of METTL3, YTHDF2, or YTHDF3, as levels of these proteins remained consistent following lytic reactivation in TREX-BCBL1, iSLK.219, and iSLK.BAC16 cells (**Fig 10**). Furthermore, we also checked whether the subcellular localization of YTHDF2 might vary between cell lines. Unexpectedly, we detected YTHDF2 in both the nucleus and cytoplasm upon fractionation of uninduced and induced lysates (**Fig 11**). However, we did not notice a dramatic difference in subcellular localization of YTHDF2 between iSLK.BAC16 and TREX-BCBL-1 cells, regardless of their reactivation state.

Finally, to determine whether the m^6A pathway components impacted the outcome of the viral lifecycle in TREX-BCBL1 cells, we measured the impact of METTL3, YTHDF2, and YTHDF3 protein knockdown on virion production using a supernatant transfer assay. TREX-BCBL-1 cells lack the viral GFP marker, and thus infection of recipient cells was instead measured by RT-qPCR for the KSHV latency-associated LANA transcript. Again in contrast to the iSLK cell data, we observed that METTL3, YTHDF2, and YTHDF3 were dispensable for virion production in TREX-BCBL-1 cells (**Fig 12E**). Instead, METTL3 depletion consistently resulted in a modest, though not statistically significant, increase in the level of LANA mRNA in the recipient cells (**Fig 12E**). In summary, METTL3 and YTHDF2 appear to function in a pro-viral capacity and promote ORF50 expression in iSLK.219 and iSLK.BAC16 cells, but instead restrict ORF50 expression in TREX-BCBL-1 cells. These findings highlight how at least a subset of m^6A pathway functions and targets may diverge between cell types.

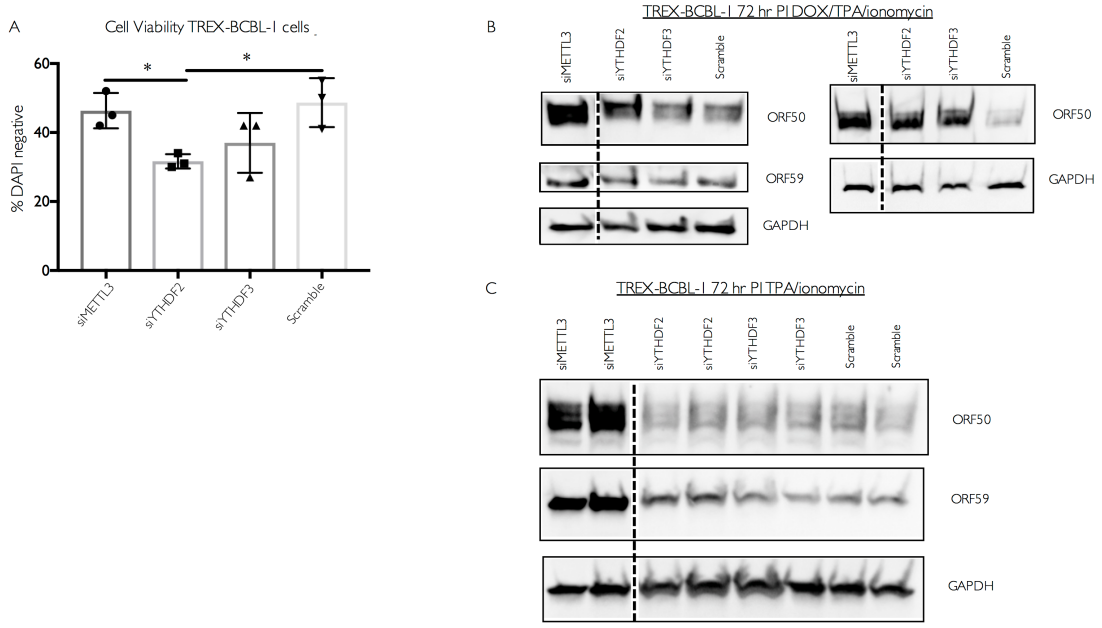

Fig 9. Impact of writers and readers upon viability and reactivation of TREX-BCBL-1 cells
(A) Quantification of cell viability following siRNA nucleofection and reactivation in TREX-BCBL-1 cells. TREX-BCBL-1 cells were nucleofected twice with the indicated siRNAs as described in the methods, and then reactivated for 36 hr with dox, PMA and ionomycin. Cells were collected and diluted 1:1 with Trypan blue prior to counting on a Countess II Automated Cell Counter. Viability from three independent experiments is depicted in the bar graphs. Unpaired Student's t test was used to evaluate the statistical difference between samples. Significance is shown for P values <0.05 (*). (B) Western blots from replicate experiments showing viral ORF50 and ORF59 protein levels in TREX-BCBL-1 cells treated with the indicated siRNAs and reactivated with dox, TPA, and ionomycin as described in Fig. 6C. (C) Western blots showing viral ORF50 and ORF59 protein levels in TREX-BCBL-1 cells treated with the indicated siRNAs for 72 hr prior to reactivation with TPA and ionomycin. Note the dotted line indicates where intervening bands were cropped out.

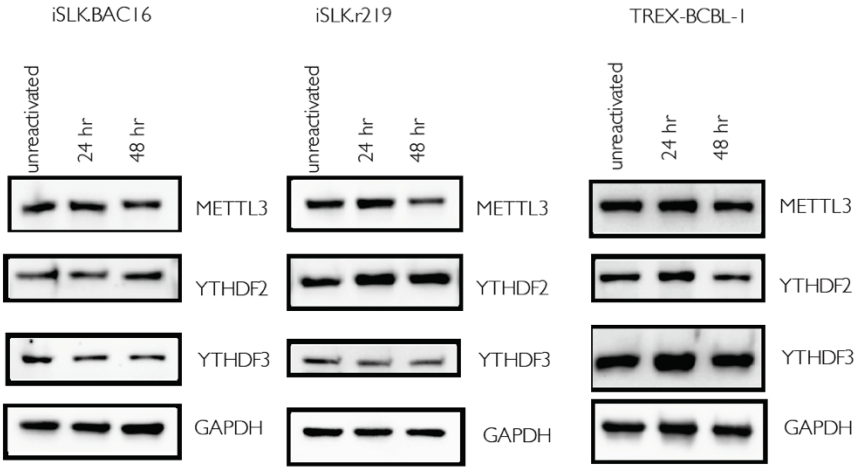

Fig 10. No changes in the levels of writers and readers following KSHV lytic reactivation
iSLK.BAC16, iSLK.219 or TREX-BCBL-1 cells were reactivated where indicated with dox for 24 or 48 hr, at which point cells were harvested and lysates were analyzed by Western blot for METTL3, YTHDF2, YTHDF3, and the GAPDH loading control.

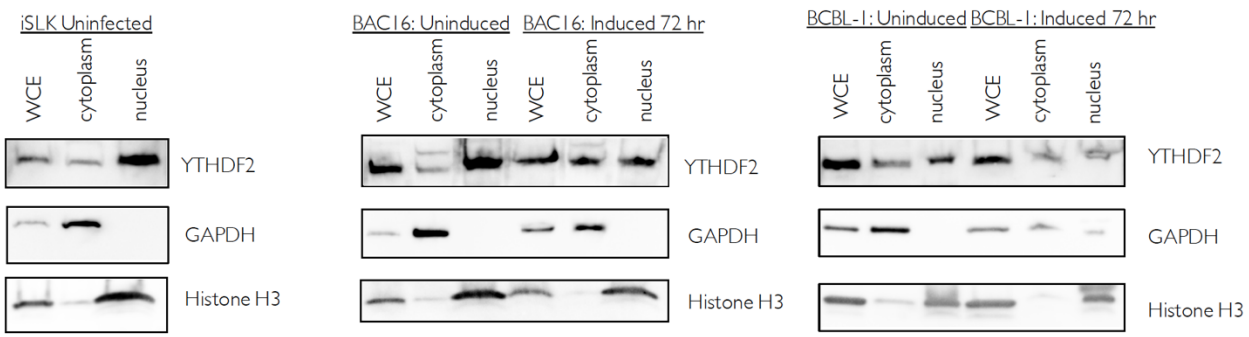

Fig 11. YTHDF2 is expressed in the cytoplasm and nucleus in iSLK.BAC16 and TREX-BCBL-1 cells iSLK.BAC16 or TREX-BCBL-1 cells were either untreated or induced where indicated with dox and sodium butyrate for 72 hr, at which point cells were harvested and Whole Cell Extract (WCE), cytoplasmic, and nuclear lysates were generating using an Ambion PARIS cell fractionation kit (Thermo Fisher). Unreactivated iSLK.RTA cells were used for iSLK uninfected blot. Lysates were analyzed by Western blot for YTHDF2, GAPDH (cytoplasmic loading control) and Histone H3 (nuclear loading control).

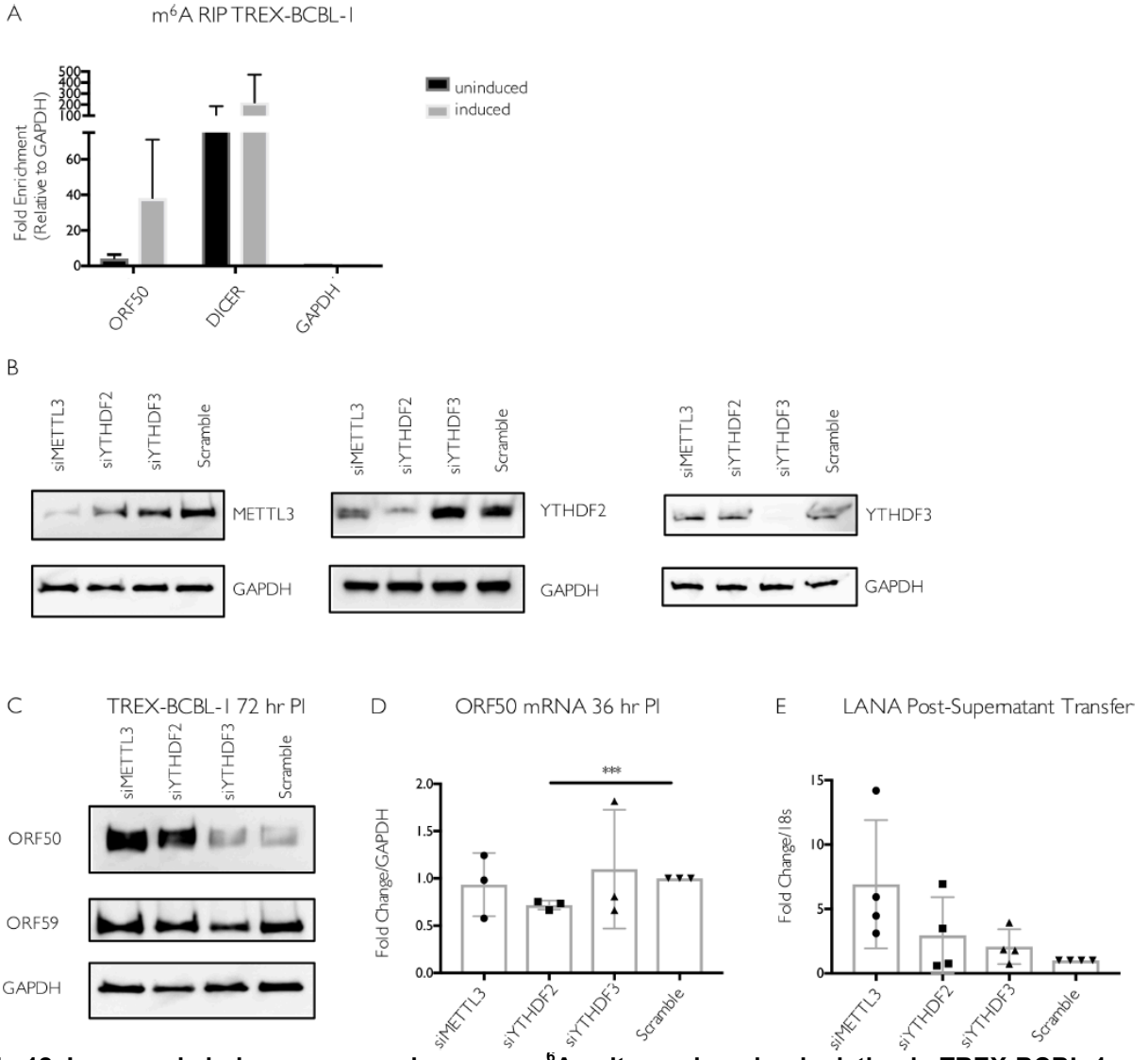

Fig 12. Increased viral gene expression upon m^{6}A writer and reader depletion in TREX-BCBL-1 cells. (A) TREX-BCBL-1 cells were reactivated with dox for 72 hr, then total RNA was isolated and subjected to m^{6}A RIP, followed by RT-qPCR for analysis of KSHV ORF50, GAPDH, and DICER. Values are displayed as fold change over input, normalized to the GAPDH negative control. Data are included from 3 biological replicates. (B-D) TREX-BCBL-1 cells were nucleofected with control scramble (scr) siRNAs or siRNAs specific to METTL3, YTHDF2, or YTHDF3, then lytically reactivated by treatment with dox, TPA and ionomycin for 72 hr. (B) Knockdown efficiency of the m^{6}A proteins relative to the loading control GAPDH was visualized by western blot. (C) Levels of the KSHV ORF50 and ORF59 proteins were assayed by western blot in the control and m^{6}A protein-depleted samples. Additional replicates are shown in **Fig 9**. (D) ORF50 gene expression was analyzed by RT-qPCR from cells treated with the indicated siRNAs and reactivated for 36 hr with dox, TPA and ionomycin. (E) Viral supernatant from the reactivated control or m^{6}A protein depleted TREX-BCBL-1 cells was transferred to uninfected HEK293T recipient cells, whereupon transfer of infection was quantified by RT-qPCR for the viral LANA transcript 48 hr post supernatant transfer. Individual data points represent 3 independent experiments. Unpaired Student's t test was used to evaluate the statistical difference between samples. Significance is shown for P values <0.05, with *** representing P value $\leq$ 0.001.

Discussion

Although m^6A modification of viral RNAs has been recognized for more than 40 years, only recently are the contributions of this epitranscriptomic mark towards viral life cycles beginning to be revealed. Thus far, global epitranscriptomic analyses have documented m^6A deposition during infections with KSHV, SV40, HIV, Influenza A virus and several members of the *Flaviviridae*, with a diverse set of resulting pro- and anti-viral roles [40,41,47,88,89,91,99,111]. The breadth and occasionally apparently contrasting functions for the m^6A pathway during infection are perhaps unsurprising given the dynamic role for this modification in controlling mRNA fate and its ability to impact virtually every stage of host gene expression [14,90]. Our global analysis of the m^6A epitranscriptome during lytic infection with the DNA virus KSHV showed the presence of m^6A across multiple kinetic classes of viral transcripts and a general decrease in m^6A deposition on cellular mRNAs. In the widely used KSHV-positive cell lines iSLK.219 and iSLK.BAC16, we found that depletion of several components of the m^6A pathway inhibited the KSHV lytic cycle, most notably in iSLK.219 cells by restricting accumulation of the viral lytic transactivator ORF50. The YTHDF2 reader protein proved particularly important, as its depletion eliminated lytic entry and virion production. These observations are suggestive of a pro-viral role for m^6A in the iSLK.219 and iSLK.BAC16 KSHV reactivation models. However, m^6A marks on mRNA in a cell are widespread and contribute to a large variety of cellular and pathogenic processes that likely occur in a cell type or context-dependent manner. In this regard, it is notable that a distinct set of phenotypes was observed for m^6A pathway components in the B cell line TREX-BCBL-1. Here, depletion of METTL3 and YTHDF2 increased ORF50 abundance, more suggestive of an anti-viral role. Thus, although KSHV engages the m^6A pathway in multiple cell types, these findings underscore the importance of not broadly extrapolating m^6A roles from a particular cell type, as this complex regulatory pathway can functionally vary in a cell type dependent manner.

What might be the basis for these phenotypic differences between cell types in the context of KSHV infection? m^6A deposition was also recently reported in many KSHV mRNAs in BCBL-1 cells, including ORF50 [71]. Furthermore, while this work was in revision, Tan and colleagues documented extensive modification of KSHV transcripts during latent KSHV infection of multiple cell types, as well as upon lytic infection of iSLK.BAC16 and TREX-BCBL-1 cells [111]. Notably, while numerous differences were found in the cellular m^6A profiles between the two cell lines, many peaks in viral transcripts were consistent across cell types, including two out of three m^6A peaks in ORF50 [111]. In agreement with these studies, we also observed extensive modification of KSHV mRNAs, and observed that ORF50 is modified in iSLK.BAC16 cells, iSLK.219 cells and TREX-BCBL-1 cells. Thus, it is not the case that the viral mRNAs engage the m^6A methyltransferase machinery in one cell type but not the other, although it is clear that site specificity of m^6A deposition, particularly in host mRNAs, can vary between cell lines. The facts that m^6A deposition is dynamic and does not strictly occur on consensus motifs render this possibility challenging to resolve. Indeed, how m^6A deposition selectively controls gene regulation on particular transcripts or under particular stimuli remains a central unanswered question in the field [14]. We hypothesize that the distinct phenotypes derive either from how the viral modifications are ‘interpreted’ in each cell type and/or indirect effects driven by an altered m^6A profile

on cellular mRNAs. The recent finding that m^{6}A modification of ORF50 in BCBL-1 cells contributes to efficient splicing through binding of YTHDC1 argues that modifications can have a direct cis-acting impact on KSHV mRNA fate [71]. However, herpesviral mRNAs are heavily reliant on host machinery at every stage of their biogenesis. Given that cellular mRNA fate is significantly altered upon depletion of METTL3 and the YTHDF reader proteins [14,37,61,62,66], it is possible that cell type specific changes in the abundance of a host factor(s) required for viral mRNA stability also contribute to the phenotypic differences. Furthermore, in HIV infected cells m^{6}A modification and YTHDF proteins have been proposed to have a combination of pro-viral and anti-viral effects, including negatively impacting reverse transcription, enhancing mRNA export, and increasing viral protein production [88,89,91]. Therefore, the m^{6}A pathway might similarly facilitate distinct phenotypes at different stages of the KSHV lifecycle.

Although our m^{6}A-seq results are in agreement with the recent report from Tan and colleagues, our data on the role of YTHDF2 in iSLK.BAC16 cells differs from theirs [111]. They did not evaluate the impact of METTL3 depletion, but reported that YTHDF2 depletion increased KSHV replication in these cells. In contrast, we observed a significant reduction in virion production upon depletion of YTHDF2 in both iSLK.219 and iSLK.BAC16 cells. Given the similarity in approaches used to evaluate the impact of YTHDF2, the basis for these differences remains unclear. However, our experiments comparing the iSLK.219 and iSLK.BAC16 cells indicates that even in cell lines of the same origin there can be differences in the m^{6}A-associated viral gene expression signatures.

As the 'interpreters' of m^{6}A marks, the individual reader proteins play prominent roles in modulating gene expression. Generally speaking, in HeLa and 293T cells, YTHDF1 binding correlates with increased translational efficiency, YTHDF2 binding accelerates mRNA decay, and YTHDF3 may serve as a cofactor to assist the other reader protein function [10,14,37,61-64]. However, other roles for these factors are rapidly emerging, particularly in the context of cell stress, infection, or in the control of specific transcripts [37,41-43,47,49,86,88,89,91]. Furthermore, m^{6}A is enriched in certain tissues, and different m^{6}A patterns have been found depending on the tissue and developmental stage [16,112]. Intriguingly, a recent study showed that hypoxia increases global m^{6}A content of mRNA, with many m^{6}A modified RNAs exhibiting increased stability, raising the possibility that m^{6}A deposition could also stabilize transcripts during other forms of cellular stress [113]. In KSHV-infected iSLK.219 cells, YTHDF2 appears essential for the post-transcriptional accumulation of ORF50, a role seemingly at odds with its more canonical mRNA destabilizing function. In this regard, it was recently revealed that SV40 late transcripts contain multiple m^{6}A sites, and that YTHDF2 strongly promotes SV40 replication [99]. Thus, YTHDF2 has been shown to play a pro-viral role in the context of both DNA and RNA viruses. Although we observed less dramatic viral gene expression phenotypes upon METTL3 depletion, it nonetheless was required for WT levels of progeny virion production in iSLK.219 and iSLK.BAC16 cells. An important consideration may be that m^{6}A factors differentially impact specific KSHV transcripts, or play different roles at distinct times during infection. However, dissecting these possibilities is likely to be complicated by the changes in ORF50 expression (either positive or negative), which will have ripple effects on the entire lytic life cycle. Another relevant question is the extent to which m^{6}A mediates its effects on

KSHV gene expression co-transcriptionally versus post-transcriptionally. A recent report indicated that m^6A is primarily installed in nascent mRNA in exons and affects cytoplasmic stability, but not splicing [87,106]. It has also been demonstrated that that m^6A can be installed co-transcriptionally, and that slowing the rate of RNA Pol II elongation enhances m^6A modification of mRNAs in a manner that ultimately decreases translation efficiency [87,106]. These add to a growing body of literature indicating that the position of m^6A in a transcript is a key feature impacting the functional consequence of the modification [14,42,43,62,64,69]. For example, m^6A in the 3' UTR has been shown to recruit YTHDF1 and enhance translation initiation in HeLa cells, while deposition of m^6A in the 5' UTR has been shown to enhance 5' cap independent translation [42,43,62]. Whether these position-linked effects on translation extend to viral transcripts remains to be tested, although there does not appear to be a consistent enrichment in a particular region of viral mRNAs for the viruses analyzed thus far. In KSHV, m^6A sites are found throughout viral ORFs, some of which also overlap with untranslated regions of other viral transcripts. As KSHV transcription depends on the host RNA Pol II, the speed of transcriptional elongation on viral mRNAs likely impacts co-transcriptional deposition and positioning of m^6A, and thus may ultimately regulate translation efficiency of a given mRNA. Thus, in the context of KSHV reactivation, a wide variety of mechanisms exist through which m^6A modification could impact the transcription and translation of viral mRNA. Deciphering these remains an important challenge for future studies, as we are currently in the early stages of understanding how this and other viruses interface with the m^6A RNA modification pathway.

Materials and Methods

Cell culture. The renal carcinoma cell line iSLK.puro containing a doxycycline-inducible copy of ORF50, and the KSHV infected renal carcinoma cell lines iSLK.219 and iSLK.BAC16 bearing doxycycline-inducible ORF50 [101] were cultured in Dulbecco's modified Eagle medium (DMEM; Invitrogen) with 10% fetal bovine serum (FBS; Invitrogen, HyClone) and 100 U/ml penicillin-streptomycin (Invitrogen). The KSHV-positive B cell line TREX-BCBL-1 containing a doxycycline-inducible version of ORF50 [110] was cultured in RPMI medium (Invitrogen) supplemented with 20% FBS, 100 U/ml penicillin/streptomycin, and 200 μM L-glutamine (Invitrogen). HEK293T cells (ATCC) were grown in DMEM (Invitrogen) supplemented with 10% FBS. To induce lytic reactivation of iSLK.219 cells, $2x10^6$ cells were plated in a 10 cm dish with 1 μg/ml doxycycline (BD Biosciences) and 1 mM sodium butyrate for 72 hr. Lytic reactivation of TREX-BCBL-1 cells was achieved by treatment of $7x10^5$ cells/ml with 20 ng/ml 2-O-tetradecanoylphorbol-13-acetate (TPA, Sigma), 1 μg/ml doxycycline (BD Biosciences), and 500 ng/ml ionomycin (Fisher Scientific) for 72 hr (western Blot blots for viral gene expression), or for 120 hr (supernatant transfer experiments).

siRNA experiments. For iSLK.219 cells, 100 pmol of siRNA was reverse transfected into $5x10^5$ cells plated in a 6-well dish using Lipofectamine RNAimax (Life Technologies). 24 hr post transfection, cells were trypsinized and re-seeded on a 10 cm plate. The next day, a second transfection was performed on the expanded cells with the same concentration of siRNA (400 pmol siRNA and $2x10^6$ cells). The following day, cells were lytically reactivated in a 10 cm plate. 24 hr post-reactivation, cells were lysed in RIPA buffer (10 mM Tris-Cl (pH 8.0), 1 mM EDTA, 1% Triton X-100, 0.1% sodium deoxycholate, 0.1% SDS, 140 mM NaCl) to evaluate knockdown efficiency. siRNA experiments in iSLK.BAC16 cells were conducted with the same siRNAs and concentrations. For experiments to assess mRNA and protein levels at 24 hr post-reactivation, one round of siRNA knockdown was performed 48 hr prior to reactivation, and knockdown efficiency was evaluated at the time of cell harvest. For iSLK.BAC16 supernatant transfer experiments, two rounds of siRNA treatment were used, as described for iSLK.219 cells.

For TREX-BCBL-1 cells, 200 pmol of siRNA was nucleofected into $2x10^6$ cells using Lonza Cell Line Nucleofector Kit V and a Lonza Nucleofector 2b set to Program T001. After nucleofection, cells were immediately resuspended in 2.2 ml of RPMI media in a 12 well plate. 48 hr later, 200 pmol of siRNA was added again to $2x10^6$ cells using the same protocol. 48 hr after the second transfection, cells were lysed in RIPA buffer and knockdown efficiency was analyzed by Western Blot. Cell viability post-nucleofection was assessed using a Countess II Automated Cell Counter (Life Technologies) with Trypan blue staining. For RT-qPCR experiments, two rounds of siRNA knockdown were performed under the identical conditions, except using an Invitrogen Neon Nucleofector with a single pulse of 1350 volts and pulse length of 40 ms.

The following Qiagen siRNAs were used: SI00764715 and SI04279121 targeting YTHDF1, SI04205761 targeting YTHDF3, custom siRNA targeting METTL3 (sequence targeted: CTGCAAGTATGTTCACTATGA). The following Dharmacon siRNAs were used: SMARTpool siGENOME (M-021009-01-0005), targeting YTHDF2, and siGENOME Non-Targeting siRNA Pool #1 (D0012061305). These same siRNAs were used in all three cell lines for the experiments in Figs 4-12. In addition, independent

siRNAs (Qiagen SI04174534 targeting YTHDF2, Qiagen SI00764778 targeting YTHDF3 and Qiagen SI03650318 (negative control siRNA)) were used in **Fig 3**.

Supernatant transfer assay and quantification of virion production. Assays were performed as previously described [9]. Briefly, for iSLK.219 and iSLK.BAC16 cells, viral supernatant was collected 72 hr post-reactivation, filtered, and added to uninfected HEK293T cells by spinfection (1500 rpm, 90 minutes at room temperature). 12 hr later, supernatant was removed and replaced with fresh media, whereupon the cells were assessed for the successful transfer of the GFP-containing KSHV BAC 24 hr post-infection using a BD Accuri C6 flow cytometer. Briefly, cells were trypsinized, fixed in 4% paraformaldehyde, washed twice in PBS and resuspended in FACS Buffer (PBS with 1% FBS). Uninfected HEK293T cells were used to define the GFP negative population. The percentage of GFP expressing cells was quantified using FlowJo Software (FlowJo LLC). For virus produced in TREX-BCBL-1 cells, supernatant transfers were performed as in iSLK.219 cells, except the virus was transferred to HEK293T cells at 120 hr post-reactivation. To quantify virus produced in TREX-BCBL-1 cells, RNA was extracted from HEK293T cells 48 hr post-supernatant transfer, and viral gene expression was quantified by RT-qPCR using primers specific for LANA.

Affinity purification and Western blotting. Cell lysate was collected and analyzed as previously described [9]. Briefly, iSLK.219, iSLK.BAC16 or TREX-BCBL-1 cells were trypsinized, washed with PBS and lysed in RIPA buffer with protease inhibitors. After washing, 4X Laemmli sample buffer (Bio-Rad) was added to samples to elute bound proteins. Lysates were resolved by SDS-PAGE and western blots were carried out with the following antibodies: rabbit ORF50 (gift of Yoshihiro Izumiya, UC Davis), rabbit α-K8.1 (1:10000, antibody generated for this study), rabbit α-ORF59 (1:10000, antibody generated for this study), rabbit α-METTL3 (Bethyl, 1:1000), rabbit α-YTHDF1 (Proteintech, 1:1000), rabbit α-YTHDF2 (Millipore, 1:1000), rabbit α-YTHDF3 (Sigma, 1:1000), and goat α-mouse and goat α-rabbit HRP secondary antibodies (1:5000; Southern Biotech).

4sU Labeling. Following siRNA knockdown and 24 hr reactivation, iSLK.219 cells were pulse labeled with DMEM containing 500 μM 4sU (Sigma) for 30 minutes, followed by PBS wash and immediate isolation of total RNA with TRIzol. 4sU isolation was performed as previously described [114]. 4sU isolated RNA was analyzed by RT-qPCR.

RT-qPCR. Total RNA was harvested using TRIzol following the manufacturer's protocol. Samples were DNase treated using Turbo DNase (Ambion), and cDNA was synthesized from 2 μg of total RNA using AMV reverse transcriptase (Promega), and used directly for quantitative PCR (qPCR) analysis with the DyNAmo ColorFlash SYBR green qPCR kit (Thermo Scientific). All qPCR results were normalized to levels of 18S or GAPDH as indicated, and WT or scramble control set to 1. RT-qPCR primers used in this study are listed in **Table 3**.

LC-MS/MS analysis of m^6A. Total RNA was isolated from iSLK219 cells with TRIzol reagent. Dynabeads mRNA purification kit (Ambion) was used to isolate polyA(+) RNAs from 100 μg of total RNA according to the manufacturer. 100-200 ng of polyadenylated RNA was spiked with 10 μM of 5-fluorouridine (Sigma) and digested by nuclease P1 (1

U) in 25 µL of buffer containing 25 mM NaCl and 2.5 mM $ZnCl_2$ at 42 °C for 2-4 hr, followed by addition of NH_4HCO_3 (1 M, 3 µL) and bacterial alkaline phosphatase (1 U) and incubation at 37 °C for 2 hr. The sample was then filtered (Amicon 3K cutoff spin column), and 5 µL of the flow through was analyzed by liquid chromatography (LC) coupled to an Orbitrap-XL mass spectrometer (MS) equipped with an electrospray ionization source (QB3 Chemistry facility).

m^6A-RIP and m^6A-RIP-sequencing. Total cellular RNA (containing KSHV RNA) was extracted and purified by TRIzol and then DNAse treated with Turbo DNase (Ambion). 30 µl protein G magnetic beads (Invitrogen) were blocked in 1% BSA solution for 1 hour, followed by incubation with 12.5 µg affinity-purified anti-m^6A polyclonal antibody (Millipore) at 4°C for 2 hr with head-over-tail rotation. 100 µg purified RNA was added to the antibody-bound beads in IP buffer (150 mM NaCl, 0.1% NP-40, and 10 mM Tris-HCl [pH 7.4]) containing RNAse inhibitor and protease inhibitor cocktail and incubated overnight at 4°C with head-over-tail rotation. The beads were washed three times in IP buffer, and then RNA was competitively eluted with 6.7 mM m^6A-free nucleotide solution (Sigma Aldrich). RNA in the eluate was phenol chloroform extracted and then reverse transcribed to cDNA for Real-Time qPCR analysis.

High-throughput sequencing of the KSHV methylome (m^6A-seq) was carried following the previously published protocol [115]. In brief, 2.5 mg total cellular RNA was prepared from iSLK.219 cells that were either unreactivated, or reactivated for five days with doxycycline. RNA was isolated and DNAse treated as in the m^6A RIP, except the RNA was first fragmented to lengths of ~100 nt prior to immunoprecipitation with anti-m^6A antibody (Synaptic Systems). Immunoprecipitated RNA fragments and comparable amounts of input were subjected to first-strand cDNA synthesis using the NEBNext Ultra RNA Library Prep Kit for Illumina (New England Biolabs). Sequencing was carried out on Illumina HiSeq2500 according to the manufacturer's instructions, using 10 pM template per sample for cluster generation, TruSeq SR Cluster kit v3 (Illumina), TruSeq SBS Kit v3-HS (Illumina) and TruSeq Multiplex Sequencing primer kit (Illumina). A reference human transcriptome was prepared based on the University of California, Santa Cruz (UCSC) and a reference KSHV transcriptome based on KSHV 2.0 annotation [116]. Analysis of m^6A peaks was performed using the model-based analysis of ChIP-seq (MACS) peak-calling algorithm. Peaks were considered significant if their MACS-assigned fold change was greater than four and individual FDR value less than 5%. Sequencing data are available on GEO repository (accession number GSE104621). Raw reads and alignment to the viral genome are shown in **Table 2**.

Statistical Analysis: All results are expressed as means +/- S.E.M. of experiments independently repeated at least three times, except where indicated. Unpaired Student's t test was used to evaluate the statistical difference between samples. Significance was evaluated with P values <0.05.

Tables

peak_start	peak_end	feature_start	feature_end	name	strand	dmTSS	dmPE	Fold Change
1690	1835	1127	2779	ORF4	+	635	1017	4.82669
17248	17536	17242	17856	vIL6	-	464	150	4.92725
28634	29143	28616	29690	PAN	+	272	802	2.66531
28634	29143	28655	28768	1.1	+	56	57	2.66531
28634	29143	28831	28965	1.2	+	67	67	2.66531
28634	29143	28888	28965	1.3	+	38	39	2.66531
29212	29645	28616	29690	PAN	+	812	262	3.19966
73092	73233	71412	74445	ORF50	+	1750	1283	3.8636
131004	131141	130876	134766	ORF75	-	3694	196	4.0544

Table 1.1 m^6A Fold Change>2 peaks in **first uninduced replicate** KSHV iSLK.219 cells. dmTSS= distance from middle of peak to Translation Start Site. dmPE= distance from middle of peak to end. Peak start and peak end refer to the locations within the KSHV BAC16 genome.

peak_start	peak_end	feature_start	feature_end	name	strand	dmTSS	dmPE	Fold Change
709	827	105	959	ORFK1	+	663	191	2.6428
1673	1876	1127	2779	ORF4	+	647	1005	5.07048
17255	17515	17242	17856	vIL6	-	471	143	2.59748
28632	29644	28616	29690	PAN	+	522	552	2.33256
28632	29644	28655	28768	1.1	+	56	57	2.33256
28632	29644	28831	28965	1.2	+	67	67	2.33256
28632	29644	28888	28965	1.3	+	38	39	2.33256
73692	73820	71412	74445	ORF50	+	2344	689	2.30481
124451	124563	124252	127623	ORF73	-	3116	255	2.0234

Table 1.2 m^6A Fold Change>2 peaks in **second uninduced replicate** KSHV iSLK.219 cells. dmTSS= distance from middle of peak to Translation Start Site. dmPE= distance from middle of peak to end. Peak start and peak end refer to the locations within the KSHV BAC16 genome.

peak_start	peak_end	feature_start	feature_end	name	strand	dmTSS	dmPE	Fold Change
15622	15815	14500	15756	ORF10	+	1189	67	3.44245
15622	15815	15574	15756	ORF10.2	+	115	67	3.44245
15622	15815	15633	15722	ORF11.1	+	44	45	3.44245
15622	15815	15648	15722	ORF11.2	+	37	37	3.44245
15622	15815	15771	16994	ORF11	+	22	1201	3.44245
16163	16358	15771	16994	ORF11	+	489	734	2.50834

16697	16996	15771	16994	ORF11	+	1074	149	3.30707
17198	18121	17242	17856	vIL6	-	307	307	6.98696
17198	18121	17602	18534	ORF2	-	673	259	6.98696
17198	18121	17877	17915	vIL6.5	-	19	19	6.98696
17198	18121	17902	18003	vIL6.4	-	51	50	6.98696
17198	18121	17985	18047	vIL6.3	-	31	31	6.98696
17198	18121	18057	18116	vIL6.1	-	30	29	6.98696
18703	19051	18589	19128	ORFK3A	-	251	288	4.89438
18703	19051	18589	19557	ORFK3	-	680	288	4.89438
18703	19051	18589	19128	ORFK3A	-	251	288	4.89438
19233	19351	18589	19557	ORFK3	-	265	703	2.34715
21316	21931	21274	22864	ORFK4.1	-	1241	349	5.77533
21316	21931	21495	21779	ORFK4	-	142	142	5.77533
21316	21931	21743	21820	ORFK4A	-	39	38	5.77533
24189	24892	24871	24915	1.4KbB	+	10	34	7.11182
25631	25942	25663	26433	ORFK5	-	631	139	3.31605
26073	26497	25663	26433	ORFK5	-	180	590	2.17692
28507	29671	28616	29690	PAN	+	527	547	6.86332
28507	29671	28655	28768	1.1	+	56	57	6.86332
28507	29671	28831	28965	1.2	+	67	67	6.86332
28507	29671	28888	28965	1.3	+	38	39	6.86332
30165	30351	29962	30489	ORF16	+	296	231	3.71139
30715	30915	30369	32243	ORF17	-	1428	446	2.1272
30715	30915	30639	31505	ORF17.5	-	690	176	2.1272
31002	31524	30369	32243	ORF17	-	980	894	5.05684
31002	31524	30639	31505	ORF17.5	-	252	614	5.05684
35115	35411	35201	36943	ORF21	+	105	1637	4.59207
35115	35411	34429	35202	ORF20B	-	44	729	4.59207
35115	35411	34429	35322	ORF20A	-	104	789	4.59207
42564	42679	42595	46725	ORF25	+	42	4088	2.29871
42961	43123	42595	46725	ORF25	+	447	3683	3.00001
50888	51008	50580	51524	ORF31	+	368	576	2.23334
52847	53247	52578	53582	ORF33	+	469	535	3.13861
58482	58649	57089	58549	ORF37	+	1426	34	3.11006
58482	58649	58455	58589	ORF38.2	+	80	54	3.11006
58482	58649	58504	58689	ORF38	+	72	113	3.11006
58482	58649	54708	67074	ORF44	+	3857	8509	3.11006
67582	67985	67169	68392	ORF45	-	609	614	2.24823
67582	67985	67140	68952	ORF45.1	+	643	1169	2.24823
68377	68636	67169	68392	ORF45	-	8	1215	2.68519

68377	68636	68364	68447	ORF45.1	-	35	48	2.68519
68377	68636	68453	69220	ORF46	-	676	91	2.68519
68377	68636	67140	68952	ORF45.1	+	1366	446	2.68519
72388	72492	71412	74445	ORF50	+	1028	2005	2.577
72388	72492	72384	72425	ORF49.1	-	19	22	2.577
73029	73481	71412	74445	ORF50	+	1843	1190	5.05064
73668	73839	71412	74445	ORF50	+	2341	692	2.74664
74123	74437	71412	74445	ORF50	+	2868	165	3.26211
74123	74437	74130	74222	ORF50AS	-	46	46	3.26211
75791	75983	75731	76511	ORFK8.1	+	156	624	2.26493
75791	75983	75890	75971	short	+	40	41	2.26493
76279	76507	75731	76511	ORFK8.1	+	662	118	5.15611
76630	76941	76618	77013	ORF52	-	228	167	3.63089
77362	77479	77149	77481	ORF53	-	61	271	3.21707
81835	81964	81886	83361	ORF57	+	39	1436	3.38962
82021	82219	81886	83361	ORF57	+	234	1241	2.92941
82287	83023	81886	83361	ORF57	+	769	706	6.22493
95394	95608	95368	96558	ORF59	-	1057	133	2.17696
96468	96580	95368	96558	ORF59	-	45	1145	2.26902
111712	112029	103819	111726	ORF64	+	7900	7	2.27925
111712	112029	111750	112262	ORF65	-	373	139	2.27925
112177	112331	111750	112262	ORF65	-	43	469	3.84497
112177	112331	112289	112321	ORF65.1	-	16	16	3.84497
113695	113892	113512	114327	ORF67	-	534	281	2.59641
114201	114497	113512	114327	ORF67	-	63	752	5.20902
114201	114497	114382	114624	ORF67.5	-	185	57	5.20902
117277	117787	117738	119075	ORFK12	-	1313	24	4.1951
117277	117787	117738	119084	C2	-	1322	24	4.1951
117877	119188	117738	119075	ORFK12	-	599	738	7.11182
117877	119188	117738	119084	C2	-	604	742	7.11182
125130	125722	124252	127623	ORF73	-	2197	1174	6.46812
125884	126128	124252	127623	ORF73	-	1617	1754	2.23313

Table 1.3 m^6A Fold Change>2 peaks in **first induced replicate** KSHV iSLK.219 cells. dmTSS= distance from middle of peak to Translation Start Site. dmPE= distance from middle of peak to end. Peak start and peak end refer to the locations within the KSHV BAC16 genome.

peak_start	peak_end	feature_start	feature_end	name	strand	dmTSS	dmPE	Fold Change
13921	14042	11344	14382	ORF9	+	2637	401	2.19852
15610	15897	14500	15756	ORF10	+	1183	73	4.8592
15610	15897	15574	15756	ORF10.2	+	109	73	4.8592
15610	15897	15633	15722	ORF11.1	+	44	45	4.8592
15610	15897	15648	15722	ORF11.2	+	37	37	4.8592
15610	15897	15771	16994	ORF11	+	63	1160	4.8592
16127	16540	15771	16994	ORF11	+	562	661	3.77497
16630	17004	15771	16994	ORF11	+	1041	182	5.11784
17197	18170	17242	17856	vIL6	-	307	307	6.13178
17197	18170	17602	18534	ORF2	-	648	284	6.13178
17197	18170	17877	17915	vIL6.5	-	19	19	6.13178
17197	18170	17902	18003	vIL6.4	-	51	50	6.13178
17197	18170	17985	18047	vIL6.3	-	31	31	6.13178
17197	18170	18057	18116	vIL6.1	-	30	29	6.13178
18703	19143	18589	19128	ORFK3A	-	213	326	4.51374
18703	19143	18589	19557	ORFK3	-	634	334	4.51374
18703	19143	18589	19128	ORFK3A	-	213	326	4.51374
19242	19352	18589	19557	ORFK3	-	260	708	2.26982
21499	21884	21274	22864	ORFK4.1	-	1173	417	4.7262
21499	21884	21495	21779	ORFK4	-	140	144	4.7262
21499	21884	21743	21820	ORFK4A	-	39	38	4.7262
22713	22848	21274	22864	ORFK4.1	-	84	1506	2.84159
22713	22848	22723	22806	ORFK4.1c	-	42	41	2.84159
22713	22848	22545	22850	ORFK4.1b	-	70	235	2.84159
24187	24897	24871	24915	1.4KbB	+	13	31	6.51578
25644	25859	25663	26433	ORFK5	-	672	98	2.74627
26086	26483	25663	26433	ORFK5	-	174	596	2.47424
28504	29660	28616	29690	PAN	+	522	552	6.4288
28504	29660	28655	28768	1.1	+	56	57	6.4288
28504	29660	28831	28965	1.2	+	67	67	6.4288
28504	29660	28888	28965	1.3	+	38	39	6.4288
30164	30324	29962	30489	ORF16	+	282	245	3.6647
30717	31529	30369	32243	ORF17	-	1120	754	5.17721
30717	31529	30639	31505	ORF17.5	-	394	472	5.17721
35110	35403	35201	36943	ORF21	+	101	1641	3.98724
35110	35403	34429	35202	ORF20B	-	46	727	3.98724
35110	35403	34429	35322	ORF20A	-	106	787	3.98724
35622	35876	35201	36943	ORF21	+	548	1194	2.55387

42546	42705	42595	46725	ORF25	+	55	4075	2.1997
42939	43146	42595	46725	ORF25	+	447	3683	2.63712
46627	46856	42595	46725	ORF25	+	4081	49	2.92367
50853	51029	50580	51524	ORF31	+	361	583	2.87174
52848	53259	52578	53582	ORF33	+	475	529	3.39709
56825	56962	54708	67074	ORF44	+	2185	10181	2.29044
58524	58634	57089	58549	ORF37	+	1447	13	2.14549
58524	58634	58455	58589	ORF38.2	+	101	33	2.14549
58524	58634	58504	58689	ORF38	+	75	110	2.14549
58524	58634	54708	67074	ORF44	+	3871	8495	2.14549
59906	60019	58789	59991	ORF39	-	43	1159	2.71918
59906	60019	54708	67074	ORF44	+	5254	7112	2.71918
67212	68030	67169	68392	ORF45	-	771	452	3.09772
67212	68030	67140	68952	ORF45.1	+	481	1331	3.09772
68385	68722	67169	68392	ORF45	-	4	1219	3.77689
68385	68722	68364	68447	ORF45.1	-	31	52	3.77689
68385	68722	68453	69220	ORF46	-	633	134	3.77689
68385	68722	67140	68952	ORF45.1	+	1413	399	3.77689
68818	68924	68453	69220	ORF46	-	349	418	2.06559
68818	68924	67140	68952	ORF45.1	+	1731	81	2.06559
69181	69311	68453	69220	ORF46	-	20	747	2.1678
69181	69311	69228	69731	ORF47	-	462	41	2.1678
71918	72084	71412	74445	ORF50	+	589	2444	2.6606
71918	72084	71446	72354	ORF49	-	353	555	2.6606
72372	72512	71412	74445	ORF50	+	1030	2003	4.02646
72372	72512	72384	72425	ORF49.1	-	21	20	4.02646
72660	72766	71412	74445	ORF50	+	1301	1732	2.15852
72987	73547	71412	74445	ORF50	+	1855	1178	5.48157
73624	73942	71412	74445	ORF50	+	2371	662	3.82859
74043	74454	71412	74445	ORF50	+	2832	201	4.5723
74043	74454	74130	74222	ORF50AS	-	46	46	4.5723
75778	75942	75731	76511	ORFK8.1	+	129	651	2.06838
75778	75942	75890	75971	short	+	26	55	2.06838
76279	76503	75731	76511	ORFK8.1	+	660	120	5.57457
77315	77486	77149	77481	ORF53	-	83	249	4.35726
77315	77486	77483	78439	ORF54	+	1	955	4.35726
81827	83013	81886	83361	ORF57	+	563	912	5.53325
95378	95624	95368	96558	ORF59	-	1057	133	2.88483
96443	96590	95368	96558	ORF59	-	58	1132	2.93549
112181	112316	111750	112262	ORF65	-	41	471	3.45117

112181	112316	112289	112321	ORF65.1	-	19	13	3.45117
114233	114484	113512	114327	ORF67	-	47	768	4.49222
114233	114484	114382	114624	ORF67.5	-	191	51	4.49222
117285	117778	117738	119075	ORFK12	-	1317	20	3.12261
117285	117778	117738	119084	C2	-	1326	20	3.12261
117832	119188	117738	119075	ORFK12	-	622	715	6.51578
117832	119188	117738	119084	C2	-	626	720	6.51578
125140	125719	124252	127623	ORF73	-	2194	1177	6.31278
125862	126119	124252	127623	ORF73	-	1633	1738	2.28234

Table 1.4 m^{6}A Fold Change>2 peaks in **second induced replicate** KSHV iSLK.219 cells. dmTSS= distance from middle of peak to Translation Start Site. dmPE= distance from middle of peak to end. Peak start and peak end refer to the locations within the KSHV BAC16 genome.

% aligned to KSHV genome (BAC16)	Untrimmed reads	Trimmed reads
IP_uninduced 1	0.06%	0.06%
IP_uninduced 2	0.09%	0.09%
IP_induced 1	3.81%	3.91%
IP_induced 2	3.76%	3.87%
input_uninduced 1	0.06%	0.06%
input_uninduced 2	0.10%	0.11%
input_induced 1	7.94%	8.12%
input_induced 2	8.15%	8.34%

Table 2 Alignment of m^{6}A-seq reads to KSHV genome. The reads were analyzed using FastQC to look for adapter contamination. Following fastqc, the reads were trimmed to remove adapters. The trimmed reads were aligned to the KSHV BAC16 genome using Bowtie2.

Primer	Sequence (5'-3')	Orientation F: Forward R: Reverse
vIL6	CGGTTCACTGCTGGTATCTG	F
vIL6	CAGTATCGTTGATGGCTGGT	R
ORF57	TTTGACGAATCGAGGGACGACG	F
ORF57	GCAGTTGAGAACGACCTTGAGAT	R
ORF37	TGGGCGAGTTTATTGGTAGTGAGG	F
ORF37	CTCCACTAGACAGCAGATGTGG	R
K8.1	TCCCTAAACGGGACCAGACT	F
K8.1	ACCCAGAGGCAGACGTATCT	R
PAN	TAATGTGAAAGGAAAGCAGCGCCC	F
PAN	CATTTAGGGCAAAGTGGCCCGATT	R
vGPCR	GTGCCTTACACGTGGAACGTT	F
vGPCR	GGTGACCAATCCATTTCCAAGA	R
K1	CCAAACGGACGAAATGAAAC	F
K1	TGTGTGGTTGCATCGCTATT	R
GAPDH	CGGAGTCAACGGATTTGGTCGTAT	F
GAPDH	AGCCTTCTCCATGGTGGTGAAGAC	R
ORF50	CGCAATGCGTTACGTTGTTG	F
ORF50	GCCCGGACTGTTGAATCG	R
ORF50 viral	GAGTCCGGCACACTGTACC	F
ORF50 viral	AAACTGCCTGGGAAGTTAACG	R
DICER	TGCTATGTCGCCTTGAATGTT	F
DICER	AATTTCTCGATAGGGGTGGTCTA	R
18s	GTAACCCGTTGAACCCCATT	F
18s	CCATCCAATCGGTAGTAGCG	R
LANA	TGGCCCATCTCGCGAATA	F
LANA	AACGCGCCTCATACGAACTC	R
SON	CGACAGCGCTGGAATCCTAT	F
SON	GCCATCAAGGGATCCACTCC	R

Table 3 List of RT-qPCR primers used in this study.

Chapter 3: Perspectives and Future Directions

Diverse impact of m^{6}A modification across multiple viruses

The field of post-transcriptional RNA modifications in viruses has burgeoned in recent years. Global epitranscriptomic analyses have documented extensive m^{6}A deposition during infections with KSHV, SV40, HIV, Hepatitis B virus, Influenza A virus and several members of the *Flaviviridae* [39-41,47,88,89,91,99,111]. The specifics of how m^{6}A impacts these lifecycles have been described in several recent reviews [48,90,117,118]. To summarize, in two nuclear replicating viruses, SV40 and Influenza, m^{6}A and the reader protein YTHDF2 have been shown to play a proviral role[40,99]. In flaviviruses, an antiviral role for m^{6}A writers and readers has been demonstrated[41,47]. Yet, in the majority of cases, the underlying molecular mechanisms remain unclear. Furthermore, for several viruses with highly complex lifecycles, both pro and anti-viral roles for m^{6}A have been proposed.

An illustration of this can be found in recent studies examining HIV and Hepatitis B virus (HBV). These viruses both have complicated lifecycles, with key regulatory steps occurring in both the nucleus and cytoplasm [119,120]. Both viruses feature a reverse transcription step, although in HIV it occurs at the beginning of the viral lifecycle and in HBV it occurs near the end of the lifecycle. In HIV, reader proteins are proposed to bind methylated viral RNA in the cytoplasm and block its reverse transcription to cDNA, thus inhibiting the rest of the viral lifecycle[91]. Upon reactivation from latency, methylation of the highly structured Rev Response Element in the genomic RNA has been proposed to enhance Rev protein binding and RNA export[89]. Thus, depletion of m^{6}A writers inhibits virion production and depletion of erasers as the opposite effect. Furthermore, m^{6}A sites in the 3'UTR of HIV viral mRNA are proposed to enhance translation, with this effect observed for YTHDF1, 2, and 3[88]. In HBV, a recent study also revealed pro and anti-viral roles[39]. Depletion of m^{6}A led to reduced reverse transcription of the pgRNA, yet increased HBV protein expression. Thus, in two viruses with lifecycles involving RNA and DNA intermediates, m^{6}A is proposed to have opposing effects on discrete steps in the viral lifecycle.

Technical Challenges

Amid the varied and sometimes contradictory roles ascribed to the m^{6}A pathway in viral infection, one common theme is the enrichment of m^{6}A in the RNAs of both nuclear and cytoplasmic replicating viruses. This is intriguing given the extensive co-evolutionary history between viruses and their hosts. While m^{6}A is proposed to lead to anti-viral phenotypes in some contexts, there should be selective pressure for m^{6}A consensus sequences in viral RNA to mutate over time if they exert a substantial fitness cost to the virus [118]. Many published studies of m^{6}A in viruses have only looked at a single time point during infection, thus neglecting the fact that m^{6}A modifications are reported to be dynamic[14]. As more comprehensive studies are conducted, they will likely uncover additional roles for the m^{6}A pathway in regulating discrete phases of the viral lifecycle. In the case of KSHV, the broad enrichment of m^{6}A across multiple kinetic classes of transcripts renders it very difficult to distinguish direct effects from indirect effects. Furthermore, the asynchronous nature of lytic induction makes it challenging to

analyze the impact of a host component on a single phase of the viral lifecycle. As CRISPR/Cas9 knockouts of METTL3 and YTHDF2 may compromise cell viability, technological advancements to achieve robust, transient depletion of m^6A components will be necessary. Additionally, synonymous mutation of specific viral m^6A consensus sites could yield mechanistic insight into the site-specificity of reader protein binding, and avoid confounding effects caused by impaired cellular differentiation and/or viability.

Another limitation of existing viral m^6A-seq studies is the resolution of m^6A peaks. These studies were carried out using so-called "1^{st} generation" sequencing techniques involve the chemical fragmentation of RNA to lengths of 100 nt [115]. The m^6A antibody is then used to pull out the chemically modified transcripts. While this antibody is highly specific, the resolution of the sequencing technique is limited by the fragment size of the RNA. Therefore, we are only able to detect the approximate location of m^6A on a transcript. As such, when m^6A consensus motifs are found in close proximity to each other (as is the case for the ORF50 transcript), we are not able to discern which of the neighboring sites are modified. Furthermore, we cannot discern the exact stoichiometry of the modification (the percent modified versus unmodified) at any given consensus motif. As several studies have suggested site-specific functions for m^6A in the viral lifecycle, improved resolution is critical[39,41]. A newer method has been developed, utilizing crosslinking of RNA incubated with the anti-m^6A antibody, followed by the introduction of truncations or C-T transitions that allow mapping of specific m^6A sites [121]. This technique has the potential to significantly improve resolution of m^6A-seq studies, although not fully addressing the problem of stoichiometry. In the context of KSHV, site-specific mapping of transcripts such as ORF50 could be overlaid with CLIP-seq profiles for individual reader proteins to determine their relative binding profiles.

Cell-type specific roles for YTHDF2

It remains unclear why YTHDF2 is required for robust lytic replication in iSLK.219 and iSLK.BAC16 reactivation models, but not in TREX-BCBL-1 cells. YTHDF2 is not reported to have any intrinsic biochemical activity, instead recruiting other effector proteins to the modified mRNA [61,66]. In particular, as the closely related readers YTHDF1-3 are reported to have functional redundancy, why does YTHDF2 depletion lead to more dramatic phenotypes[66]? Published studies in other viral systems have shown roles for YTHDF2 that are both strongly pro and anti-viral [40,41,88,99,111]. However, these studies largely do not prove that YTHDF2 is acting in *cis* on viral RNA, leaving open the possibility that it is instead impacting the expression of cellular mRNAs involved in the viral replicative process. Furthermore, no other published studies have examined cell-type specific differences in YTHDF2 localization or function.

To narrow down the possibilities as to how YTHDF2 might be acting, we first examined whether differential localization or expression of YTHDF2 could explain the phenotypes observed in iSLK cells and BCBL-1 cells. We saw relatively similar expression of YTHDF2 comparing latent and lytic iSLK and BCBL-1 cell types (Fig 10). Furthermore, cell fractionation experiments revealed no gross differences in the subcellular localization, with YTHDF2 appearing in the cytoplasmic and nuclear/perinuclear fractions in both cases (Fig 11). However, as it has been proposed that depletion of one reader protein can significantly enhance the RNA binding affinity of another reader protein, even subtle differences between cell types could have a

significant impact [64]. Since all of the structure-independent readers are reported to bind to the same consensus sequence and at least partially overlap in their binding sites, differences in the stoichiometry of reader proteins binding modified transcripts could exist between cell types.

Next, we wondered whether significant differences could exist in the m^6A methylome between cell types, thus impacting which transcripts are bound by YTHDF2. Transcriptome-wide m^6A-seq revealed about 70% of viral m^6A peaks are shared between lytic iSLK.BAC16 and TREX-BCBL-1 cells[111]. While there were some intriguing differences, including a cluster of modification in the region of ORF34-37 in BCBL1 cells not found in iSLK cells, changes in the methylation of cellular transcripts were more dramatic [111]. Indeed, while the canonical GGAC motif was enriched for m^6A in both cell types, lytically reactivated iSLK.BAC16 cells exhibited increased 5' UTR methylation and slightly decreased 3'UTR methylation compared to latent cells. In contrast, lytically reactivated BCBL-1 cells exhibited decreased 5' UTR methylation and increased 3'UTR methylation [111]. However, the functional consequences of these changes remain unclear. Thus, a future direction would involve CLIP-seq for YTHDF2 and other m^6A readers in both cell types to reveal whether these changes in m^6A distribution alter reader protein binding.

As numerous cellular signaling pathways are triggered upon KSHV reactivation, changes in the methylation state of cellular transcripts could have broad impacts upon lytic gene expression. Protein Kinase A (PKA), XBP-1, CBP, the SWI/SNF chromatin remodeling complex and the TRAP/Mediator complex have all been reported to enhance lytic induction and/or gene expression[3]. In particular, a constitutively active form of Ras, v-Ki-ras2, has been shown to promote ORF50 transcriptional activity by over one hundred fold, playing a broader role in the Raf/MEK/ERK pathway [122]. In turn, NFκB suppresses AP-1 and blocks ORF50 transactivation by antagonizing the recombination signal sequence binding protein Jκ (RBP-jκ) cofactor, a major transcriptional repressor of the Notch signaling pathway, in B lymphocytes [3]. Given the role of cellular signaling pathways in amplifying and antagonizing ORF50 expression, it will be important for future studies to examine the role of YTHDF2 in regulating the stability of m^6A modified cellular transcripts. For example, if YTHDF2 binds and destabilizes the transcript of a m^6A modified cellular transcript that negative regulates ORF50 activity, that could promote ORF50 expression. Thus, cell-type specific differences in either the expression level or modification state of ORF50 cellular co-factors could potentially lead to disparate impacts upon viral reactivation.

Role of m^6A in the innate immune response

As extensive remodeling of the host transcriptome occurs upon viral infection, a key question is whether anti-viral transcripts are impacted by m^6A modification? Of particular interest in viral infection, IFN-I products induce resistance to viral infection, but also cause a variety of autoimmune diseases when their production is dysregulated[123]. Thus, expression of IFN-I transcripts must be tightly regulated. While these transcripts are known to contain AU-rich elements in their 3' UTRs to help facilitate their post-transcriptional degradation, additional mechanisms to regulate IFN-I transcript stability may exist [124]. As m^6A is suggested to destabilize transcripts, m^6A

modification of IFN-I transcripts could potentially contribute to the pro-viral effects ascribed to the m^{6}A pathway during several viral infections [40,88,99,127].

To address this possibility, two recent studies focused on the role of m^{6}A on host transcripts during infection with human cytomegalovirus (HCMV) [125,126]. Both studies confirmed the *IFNB* transcript contains multiple m^{6}A sites, and that depletion of the m^{6}A writers METTL3 and METTL14 enhanced IFN-I transcript abundance and restricted viral replication. In addition, Rubio and colleagues show that depletion of METTL14 enhanced *IFNB* transcription, while depletion of eraser ALKBH5 had the opposite effect[126]. These phenotypes could be recapitulated upon dsDNA stimulation or stimulation with a UV-inactivated virus, demonstrating that a viral protein is not redirecting m^{6}A components to host transcripts[125,126]. Winkler and colleagues also demonstrate that depletion of METTL3 and YTHDF2 led to stabilization of IFN-I transcripts, restricting replication of multiple RNA and DNA viruses[125]. Overall, these studies argue that stabilization of IFN-I transcripts upon m^{6}A depletion could contribute to the pro-viral phenotypes observed upon infection with multiple viruses[40,88,99,127]. Furthermore, these studies suggest that m^{6}A deposition on IFN-I transcripts could be a conserved host mechanism designed to negatively regulate the stability of IFN-I transcript[125,126]. As dsDNA can accumulate in the cytoplasm of senescent cells and trigger aberrant IFN-I production, tight regulation of IFN-I transcript stability helps prevent autoimmunity and allows IFN-I production to be rapidly shut off once a viral threat has been contained[126].

In our work, reactivation of iSLK.BAC16 cells upon depletion of METTL3 and YTHDF2 revealed significant defects in virion production, despite a relatively minor impact upon viral gene expression at early time points (**Fig 8**). Although we did not investigate a role for IFN-I, we observed a very similar impact upon KSHV virion production in this cell type to that observed by Winkler and colleagues during HCMV infection[125]. Along these lines, future studies should examine the extent to which m^{6}A modification of IFN-I transcripts impacts the replication of other beta and gammaherpesviruses. As such experiments would be very challenging to perform during the asynchronous lytic reactivation context of KSHV, they could instead be performed upon *de novo* infection with MHV-68 or MCMV. In preliminary experiments, depletion of writers and readers prior to infection with MHV-68 did not cause any clear changes in infectivity 24 hpi (data not shown). However, these experiments were performed in HEK293 cells, a human transformed cell line which is not a biological target of MHV-68 infection. Thus, future experiments with MHV-68 or MCMV should be performed in primary cell types with intact innate immune sensors.

Potential role of other m^{6}A readers and erasers

As m^{6}A binding proteins have been proposed to both stabilize and destabilize transcripts, this could explain why the impact of METTL3 depletion did not always phenocopy that observed upon YTHDF2 depletion (**Figs 4, 6, 8, 12**). For example, IGF2BPs are m^{6}A readers that are proposed to stabilize transcripts, and appear to have a binding profile largely distinct from that of YTHDF2[78]. Thus, RNA immunoprecipitation experiments should be performed to reveal whether these proteins bind KSHV transcripts, as well as experiments to examine their subcellular localization across cell types. Furthermore, while knockdown of each individual YTHDF protein did

not appear to greatly destabilize the expression of other YTHDF family members, future studies should examine whether depletion of YTHDF proteins also impacts the expression of other classes of m^6A readers such as the IGF2BPs.

Although the roles of the m^6A writer METTL3 and the YTH-domain reader proteins have been examined by multiple studies during KSHV lytic reactivation, little is known about the function of the m^6A erasers in the context of viral infection. The extent to which m^6A deposition can be reversible is disputed, as one study performed in a non-infectious context indicated that the m^6A content of transcripts remained largely static after mRNA export to the cytoplasm [106]. Still, it cannot be ruled out that viral infection could result in inhibition of m^6A erasers, thus contributing to the large increase in cellular m^6A content observed upon lytic reactivation of KSHV (**Fig 1B**). Studies in other infectious contexts have shown that depletion of erasers leads to the opposite phenotype from that seen upon depletion of writers [41,47,89,126]. While no studies have examined the role of the m^6A eraser ALKBH5 during the KSHV lytic cycle, one study reported that chemical inhibition of FTO slightly increased lytic replication in BCBL-1 cells[71]. In addition, a recent study revealed that FTO expression and subcellular localization varies considerably by cell type, thus offering a potential explanation for cell-type specific effects observed upon depletion of m^6A machinery [24]. Thus, it could be worthwhile to examine the subcellular localization of both ALKBH5 and FTO during lytic reactivation of iSLK and BCBL-1 cells, and analyze the impact of ALKBH5 depletion upon the viral lifecycle. As m^6A deposition is reported to facilitate mRNA export, inhibition of m^6A erasers in the nucleus could help ensure the proper nuclear export of key lytic transcripts upon KSHV reactivation.

Chapter 4: References

1. Jenkins FJ, Hoffman LJ. Overview of Herpesviruses. Infectious Causes of Cancer. New Jersey: Humana Press; 2000. pp. 33–49. doi:10.1385/1-59259-024-1:33

2. Bravender T. Epstein-Barr virus, cytomegalovirus, and infectious mononucleosis. Adolesc Med State Art Rev. 2010;21: 251–64– ix.

3. Aneja KK, Yuan Y. Reactivation and Lytic Replication of Kaposi's Sarcoma-Associated Herpesvirus: An Update. Front Microbiol. 2017;8: 19–23. doi:10.3389/fmicb.2017.00613

4. Ganem D. KSHV and the pathogenesis of Kaposi sarcoma: listening to human biology and medicine. J Clin Invest. American Society for Clinical Investigation; 2010;120: 939–949. doi:10.1172/JCI40567

5. Butler LM, Dorsey G, Hladik W, Rosenthal PJ, Brander C, Neilands TB, et al. Kaposi sarcoma-associated herpesvirus (KSHV) seroprevalence in population-based samples of African children: evidence for at least 2 patterns of KSHV transmission. J Infect Dis. 2009;200: 430–438. doi:10.1086/600103

6. Hair JR, Lyons PA, Smith KGC, Efstathiou S. Control of Rta expression critically determines transcription of viral and cellular genes following gammaherpesvirus infection. J Gen Virol. Microbiology Society; 2007;88: 1689–1697. doi:10.1099/vir.0.82548-0

7. Wu TT, Usherwood EJ, Stewart JP, Nash AA, Sun R. Rta of Murine Gammaherpesvirus 68 Reactivates the Complete Lytic Cycle from Latency. J Virol. 2000;74: 3659–3667. doi:10.1128/JVI.74.8.3659-3667.2000

8. Gradoville L, Gerlach J, Grogan E, Shedd D, Nikiforow S, Metroka C, et al. Kaposi's Sarcoma-Associated Herpesvirus Open Reading Frame 50/Rta Protein Activates the Entire Viral Lytic Cycle in the HH-B2 Primary Effusion Lymphoma Cell Line. J Virol. American Society for Microbiology; 2000;74: 6207–6212. doi:10.1128/JVI.74.13.6207-6212.2000

9. Davis ZH, Verschueren E, Jang GM, Kleffman K, Johnson JR, Park J, et al. Global mapping of herpesvirus-host protein complexes reveals a transcription strategy for late genes. Molecular Cell. 2015;57: 349–360. doi:10.1016/j.molcel.2014.11.026

10. Fu Y, Dominissini D, Rechavi G, He C. Gene expression regulation mediated through reversible m^{6}A RNA methylation. Nat Rev Genet. 2014;15: 293–306. doi:10.1038/nrg3724

11. Meyer KD, Jaffrey SR. The dynamic epitranscriptome: N6-methyladenosine and

gene expression control. Nat Rev Mol Cell Biol. 2014;15: 313–326. doi:10.1038/nrm3785

12. Karikó K, Buckstein M, Ni H, Weissman D. Suppression of RNA recognition by Toll-like receptors: the impact of nucleoside modification and the evolutionary origin of RNA. Immunity. 2005;23: 165–175. doi:10.1016/j.immuni.2005.06.008

13. Nachtergaele S, He C. Chemical Modifications in the Life of an mRNA Transcript. Annu Rev Genet. 2018. doi:10.1146/annurev-genet-120417-031522

14. Roundtree IA, Evans ME, Pan T, He C. Dynamic RNA Modifications in Gene Expression Regulation. Cell. 2017;169: 1187–1200. doi:10.1016/j.cell.2017.05.045

15. Yang X, Yang Y, Sun B-F, Chen Y-S, Xu J-W, Lai W-Y, et al. 5-methylcytosine promotes mRNA export - NSUN2 as the methyltransferase and ALYREF as an m5C reader. Cell Research. Nature Publishing Group; 2017;27: 606–625. doi:10.1038/cr.2017.55

16. Dominissini D, Moshitch-Moshkovitz S, Schwartz S, Salmon-Divon M, Ungar L, Osenberg S, et al. Topology of the human and mouse m6A RNA methylomes revealed by m6A-seq. Nature. 2012;485: 201–206. doi:10.1038/nature11112

17. Carlile TM, Rojas-Duran MF, Gilbert WV. Pseudo-Seq: Genome-Wide Detection of Pseudouridine Modifications in RNA. Meth Enzymol. Elsevier; 2015;560: 219–245. doi:10.1016/bs.mie.2015.03.011

18. Dai Q, Moshitch-Moshkovitz S, Han D, Kol N, Amariglio N, Rechavi G, et al. Nm-seq maps 2'-O-methylation sites in human mRNA with base precision. Cell Research. Nature Publishing Group; 2017;14: 695–698. doi:10.1038/nmeth.4294

19. Karijolich J, Yi C, Yu Y-T. Transcriptome-wide dynamics of RNA pseudouridylation. Nat Rev Mol Cell Biol. 2015;16: 581–585. doi:10.1038/nrm4040

20. Ge J, Yu Y-T. RNA pseudouridylation: new insights into an old modification. Trends Biochem Sci. 2013;38: 210–218. doi:10.1016/j.tibs.2013.01.002

21. Schwartz S, Bernstein DA, Mumbach MR, Jovanovic M, Herbst RH, León-Ricardo BX, et al. Transcriptome-wide mapping reveals widespread dynamic-regulated pseudouridylation of ncRNA and mRNA. Cell. 2014;159: 148–162. doi:10.1016/j.cell.2014.08.028

22. Li X, Ma S, Yi C. Pseudouridine: the fifth RNA nucleotide with renewed interests. Curr Opin Chem Biol. 2016;33: 108–116. doi:10.1016/j.cbpa.2016.06.014

23. Karijolich J, Yu Y-T. Converting nonsense codons into sense codons by targeted

pseudouridylation. Nature. Nature Publishing Group; 2011;474: 395–398. doi:10.1038/nature10165

24. Wei J, Liu F, Lu Z, Fei Q, Ai Y, He PC, et al. Differential m6A, m6Am, and m1A Demethylation Mediated by FTO in the Cell Nucleus and Cytoplasm. Molecular Cell. 2018;71: 973–985.e5. doi:10.1016/j.molcel.2018.08.011

25. Peer E, Moshitch-Moshkovitz S, Rechavi G, Dominissini D. The Epitranscriptome in Translation Regulation. Cold Spring Harb Perspect Biol. 2018. doi:10.1101/cshperspect.a032623

26. Li X, Xiong X, Wang K, Wang L, Shu X, Ma S, et al. Transcriptome-wide mapping reveals reversible and dynamic N(1)-methyladenosine methylome. Nat Chem Biol. Nature Publishing Group; 2016;12: 311–316. doi:10.1038/nchembio.2040

27. Dominissini D, Nachtergaele S, Moshitch-Moshkovitz S, Peer E, Kol N, Ben-Haim MS, et al. The dynamic N(1)-methyladenosine methylome in eukaryotic messenger RNA. Nature. Nature Publishing Group; 2016;530: 441–446. doi:10.1038/nature16998

28. Dai X, Wang T, Gonzalez G, Wang Y. Identification of YTH Domain-Containing Proteins as the Readers for N1-Methyladenosine in RNA. Anal Chem. 2018;90: 6380–6384. doi:10.1021/acs.analchem.8b01703

29. Amort T, Rieder D, Wille A, Khokhlova-Cubberley D, Riml C, Trixl L, et al. Distinct 5-methylcytosine profiles in poly(A) RNA from mouse embryonic stem cells and brain. Genome Biol. BioMed Central; 2017;18: 1619. doi:10.1186/s13059-016-1139-1

30. Amort T, Sun X, Khokhlova-Cubberley D, Lusser A. Transcriptome-Wide Detection of 5-Methylcytosine by Bisulfite Sequencing. RNA Methylation. New York, NY: Springer New York; 2017. pp. 123–142. doi:10.1007/978-1-4939-6807-7_9

31. Squires JE, Patel HR, Nousch M, Sibbritt T, Humphreys DT, Parker BJ, et al. Widespread occurrence of 5-methylcytosine in human coding and non-coding RNA. Nucleic Acids Research. 2012;40: 5023–5033. doi:10.1093/nar/gks144

32. Khoddami V, Cairns BR. Identification of direct targets and modified bases of RNA cytosine methyltransferases. Nat Biotechnol. Nature Publishing Group; 2013;31: 458–464. doi:10.1038/nbt.2566

33. Zhao BS, Wang X, Beadell AV, Lu Z, Shi H, Kuuspalu A, et al. m(6)A-dependent maternal mRNA clearance facilitates zebrafish maternal-to-zygotic transition. Nature. 2017;542: 475–478. doi:10.1038/nature21355

34. Desrosiers R, Friderici K, Rottman F. Identification of methylated nucleosides in

messenger RNA from Novikoff hepatoma cells. PNAS. National Academy of Sciences; 1974;71: 3971–3975.

35. Liu J, Yue Y, Han D, Wang X, Fu Y, Zhang L, et al. A METTL3-METTL14 complex mediates mammalian nuclear RNA N6-adenosine methylation. Nat Chem Biol. 2014;10: 93–95. doi:10.1038/nchembio.1432

36. Du Y, Hou G, Zhang H, Dou J, He J, Guo Y, et al. SUMOylation of the m6A-RNA methyltransferase METTL3 modulates its function. Nucleic Acids Research. 2018;46: 5195–5208. doi:10.1093/nar/gky156

37. Wang Y, Li Y, Toth JI, Petroski MD, Zhang Z, Zhao JC. N6-methyladenosine modification destabilizes developmental regulators in embryonic stem cells. Nat Cell Biol. 2014;16: 191–198. doi:10.1038/ncb2902

38. Wang X, Feng J, Xue Y, Guan Z, Zhang D, Liu Z, et al. Structural basis of N(6)-adenosine methylation by the METTL3-METTL14 complex. Nature. 2016;534: 575–578. doi:10.1038/nature18298

39. Imam H, Khan M, Gokhale NS, McIntyre ABR, Kim G-W, Jang JY, et al. N6-methyladenosine modification of hepatitis B virus RNA differentially regulates the viral life cycle. Proc Natl Acad Sci USA. 2018;115: 8829–8834. doi:10.1073/pnas.1808319115

40. Courtney DG, Kennedy EM, Dumm RE, Bogerd HP, Tsai K, Heaton NS, et al. Epitranscriptomic Enhancement of Influenza A Virus Gene Expression and Replication. Cell Host Microbe. 2017;22: 377–386.e5. doi:10.1016/j.chom.2017.08.004

41. Gokhale NS, McIntyre ABR, McFadden MJ, Roder AE, Kennedy EM, Gandara JA, et al. N6-Methyladenosine in Flaviviridae Viral RNA Genomes Regulates Infection. Cell Host Microbe. 2016;20: 654–665. doi:10.1016/j.chom.2016.09.015

42. Zhou J, Wan J, Gao X, Zhang X, Jaffrey SR, Qian S-B. Dynamic m6A mRNA methylation directs translational control of heat shock response. Nature. 2015;526: 591–594. doi:10.1038/nature15377

43. Meyer KD, Patil DP, Zhou J, Zinoviev A, Skabkin MA, Elemento O, et al. 5' UTR m(6)A Promotes Cap-Independent Translation. Cell. 2015;163: 999–1010. doi:10.1016/j.cell.2015.10.012

44. Dominissini D, Moshitch-Moshkovitz S, Schwartz S, Salmon-Divon M, Ungar L, Osenberg S, et al. Topology of the human and mouse m6A RNA methylomes revealed by m6A-seq. Nature. Nature Publishing Group; 2012;485: 201–206. doi:10.1038/nature11112

45. Ping X-L, Sun B-F, Wang L, Xiao W, Yang X, Wang W-J, et al. Mammalian

WTAP is a regulatory subunit of the RNA N6-methyladenosine methyltransferase. Cell Research. 2014;24: 177–189. doi:10.1038/cr.2014.3

46. Yue Y, Liu J, Cui X, Cao J, Luo G, Zhang Z, et al. VIRMA mediates preferential m6A mRNA methylation in 3'UTR and near stop codon and associates with alternative polyadenylation. Cell Discovery. Springer US; 2018;: 1–17. doi:10.1038/s41421-018-0019-0

47. Lichinchi G, Zhao BS, Wu Y, Lu Z, Qin Y, He C, et al. Dynamics of Human and Viral RNA Methylation during Zika Virus Infection. Cell Host Microbe. 2016;20: 666–673. doi:10.1016/j.chom.2016.10.002

48. Gokhale NS, Horner SM. RNA modifications go viral. PLoS Pathog. 2017;13: e1006188. doi:10.1371/journal.ppat.1006188

49. Lin S, Choe J, Du P, Triboulet R, Gregory RI. The m6A Methyltransferase METTL3 Promotes Translation in Human Cancer Cells. Molecular Cell. Elsevier Inc; 2016;62: 335–345. doi:10.1016/j.molcel.2016.03.021

50. Choe J, Lin S, Zhang W, Liu Q, Wang L, Ramirez-Moya J, et al. mRNA circularization by METTL3–eIF3h enhances translation and promotes oncogenesis. Nature. Springer US; 2018;: 1–25. doi:10.1038/s41586-018-0538-8

51. Pendleton KE, Chen B, Liu K, Hunter OV, Xie Y, Tu BP, et al. The U6 snRNA m6A Methyltransferase METTL16 Regulates SAM Synthetase Intron Retention. Cell. 2017;169: 824–835.e14. doi:10.1016/j.cell.2017.05.003

52. Doxtader KA, Wang P, Scarborough AM, Seo D, Conrad NK, Nam Y. Structural Basis for Regulation of METTL16, an S-Adenosylmethionine Homeostasis Factor. Molecular Cell. 2018;71: 1001–1011.e4. doi:10.1016/j.molcel.2018.07.025

53. Mendel M, Chen K-M, Homolka D, Gos P, Pandey RR, McCarthy AA, et al. Methylation of Structured RNA by the m6A Writer METTL16 Is Essential for Mouse Embryonic Development. Molecular Cell. 2018;71: 986–1000.e11. doi:10.1016/j.molcel.2018.08.004

54. Jia G, Fu Y, Zhao X, Dai Q, Zheng G, Yang Y, et al. N6-methyladenosine in nuclear RNA is a major substrate of the obesity-associated FTO. Nat Chem Biol. Nature Publishing Group; 2011;7: 885–887. doi:10.1038/nchembio.687

55. Dina C, Meyre D, Gallina S, Durand E, Körner A, Jacobson P, et al. Variation in FTO contributes to childhood obesity and severe adult obesity. Nat Genet. Nature Publishing Group; 2007;39: 724–726. doi:10.1038/ng2048

56. Frayling TM, Timpson NJ, Weedon MN, Zeggini E, Freathy RM, Lindgren CM, et al. A common variant in the FTO gene is associated with body mass index and

predisposes to childhood and adult obesity. Science. American Association for the Advancement of Science; 2007;316: 889–894. doi:10.1126/science.1141634

57. Do R, Bailey SD, Desbiens K, Belisle A, Montpetit A, Bouchard C, et al. Genetic variants of FTO influence adiposity, insulin sensitivity, leptin levels, and resting metabolic rate in the Quebec Family Study. Diabetes. 2008;57: 1147–1150. doi:10.2337/db07-1267

58. Zheng G, Dahl JA, Niu Y, Fedorcsak P, Huang C-M, Li CJ, et al. ALKBH5 is a mammalian RNA demethylase that impacts RNA metabolism and mouse fertility. Molecular Cell. 2013;49: 18–29. doi:10.1016/j.molcel.2012.10.015

59. Mauer J, Luo X, Blanjoie A, Jiao X, Grozhik AV, Patil DP, et al. Reversible methylation of m6Am in the 5′ cap controls mRNA stability. Cell Research. Nature Publishing Group; 2017;541: 371–375. doi:10.1038/nature21022

60. Zhao X, Yang Y, Sun B-F, Shi Y, Yang X, Xiao W, et al. FTO-dependent demethylation of N6-methyladenosine regulates mRNA splicing and is required for adipogenesis. Cell Research. Nature Publishing Group; 2014;24: 1403–1419. doi:10.1038/cr.2014.151

61. Wang X, Lu Z, Gomez A, Hon GC, Yue Y, Han D, et al. N6-methyladenosine-dependent regulation of messenger RNA stability. Nature. 2013;505: 117–120. doi:10.1038/nature12730

62. Wang X, Zhao BS, Roundtree IA, Lu Z, Han D, Ma H, et al. N(6)-methyladenosine Modulates Messenger RNA Translation Efficiency. Cell. 2015;161: 1388–1399. doi:10.1016/j.cell.2015.05.014

63. Shi H, Wang X, Lu Z, Zhao BS, Ma H, Hsu PJ, et al. YTHDF3 facilitates translation and decay of N(6)-methyladenosine-modified RNA. Cell Research. 2017;27: 315–328. doi:10.1038/cr.2017.15

64. Li A, Chen Y-S, Ping X-L, Yang X, Xiao W, Yang Y, et al. Cytoplasmic m(6)A reader YTHDF3 promotes mRNA translation. Cell Research. 2017;27: 444–447. doi:10.1038/cr.2017.10

65. Ivanova I, Much C, Di Giacomo M, Azzi C, Morgan M, Moreira PN, et al. The RNA m(6)A Reader YTHDF2 Is Essential for the Post-transcriptional Regulation of the Maternal Transcriptome and Oocyte Competence. Molecular Cell. 2017;67: 1059–1067.e4. doi:10.1016/j.molcel.2017.08.003

66. Du H, Zhao Y, He J, Zhang Y, Xi H, Liu M, et al. YTHDF2 destabilizes m(6)A-containing RNA through direct recruitment of the CCR4-NOT deadenylase complex. Nat Commun. Nature Publishing Group; 2016;7: 12626. doi:10.1038/ncomms12626

67. Li Z, Weng H, Su R, Weng X, Zuo Z, Li C, et al. FTO Plays an Oncogenic Role

in Acute Myeloid Leukemia as a N6-Methyladenosine RNA Demethylase. Cancer Cell. 2017;31: 127–141. doi:10.1016/j.ccell.2016.11.017

68. Weng Y-L, Wang X, An R, Cassin J, Vissers C, Liu Y, et al. Epitranscriptomic m6A Regulation of Axon Regeneration in the Adult Mammalian Nervous System. Neuron. 2018;97: 313–325.e6. doi:10.1016/j.neuron.2017.12.036

69. Xiao W, Adhikari S, Dahal U, Chen Y-S, Hao Y-J, Sun B-F, et al. Nuclear m(6)A Reader YTHDC1 Regulates mRNA Splicing. Molecular Cell. 2016;61: 507–519. doi:10.1016/j.molcel.2016.01.012

70. Kasowitz SD, Ma J, Anderson SJ, Leu NA, Xu Y, Gregory BD, et al. Nuclear m6A reader YTHDC1 regulates alternative polyadenylation and splicing during mouse oocyte development. Yan W, editor. PLoS Genet. 2018;14: e1007412–28. doi:10.1371/journal.pgen.1007412

71. Ye F, Chen ER, Nilsen TW. Kaposi's Sarcoma-Associated Herpesvirus Utilizes and Manipulates RNA N6-Adenosine Methylation To Promote Lytic Replication. Longnecker RM, editor. J Virol. 2017;91: 201. doi:10.1128/JVI.00466-17

72. Lesbirel S, Viphakone N, Parker M, Parker J, Heath C, Sudbery I, et al. The m6A-methylase complex recruits TREX and regulates mRNA export. Scientific Reports. Springer US; 2018;: 1–12. doi:10.1038/s41598-018-32310-8

73. Roundtree IA, Luo G-Z, Zhang Z, Wang X, Zhou T, Cui Y, et al. YTHDC1 mediates nuclear export of N6-methyladenosine methylated mRNAs. Elife. 2017;6. doi:10.7554/eLife.31311

74. Rafalska I, Zhang Z, Benderska N, Wolff H, Hartmann AM, Brack-Werner R, et al. The intranuclear localization and function of YT521-B is regulated by tyrosine phosphorylation. Hum Mol Genet. 2004;13: 1535–1549. doi:10.1093/hmg/ddh167

75. Kretschmer J, Rao H, Hackert P, Sloan KE, Höbartner C, Bohnsack MT. The m 6A reader protein YTHDC2 interacts with the small ribosomal subunit and the 5′–3′ exoribonuclease XRN1. RNA. 2018;24: 1339–1350. doi:10.1261/rna.064238.117

76. Hsu PJ, Zhu Y, Ma H, Guo Y, Shi X, Liu Y, et al. Ythdc2 is an N(6)-methyladenosine binding protein that regulates mammalian spermatogenesis. Cell Research. 2017;27: 1115–1127. doi:10.1038/cr.2017.99

77. Huang H, Weng H, Sun W, Qin X, Shi H, Wu H, et al. Recognition of RNA N6-methyladenosine by IGF2BP proteins enhances mRNA stability and translation. Nat Cell Biol. Springer US; 2018;20: 1–18. doi:10.1038/s41556-018-0045-z

78. Huang H, Weng H, Sun W, Qin X, Shi H, Wu H, et al. Recognition of RNA N6-methyladenosine by IGF2BP proteins enhances mRNA stability and translation.

Nat Cell Biol. Springer US; 2018;: 1–18. doi:10.1038/s41556-018-0045-z

79. Liu N, Zhou KI, Parisien M, Dai Q, Diatchenko L, Pan T. N6-methyladenosine alters RNA structure to regulate binding of a low-complexity protein. Nucleic Acids Research. 2017;45: 6051–6063. doi:10.1093/nar/gkx141

80. Liu N, Dai Q, Zheng G, He C, Parisien M, Pan T. N(6)-methyladenosine-dependent RNA structural switches regulate RNA-protein interactions. Nature. 2015;518: 560–564. doi:10.1038/nature14234

81. Liu N, Pan T. N6-methyladenosine–encoded epitranscriptomics. Cell Research. 2016;23: 98–102. doi:10.1038/nsmb.3162

82. Alarcón CR, Goodarzi H, Lee H, Liu X, Tavazoie S, Tavazoie SF. HNRNPA2B1 Is a Mediator of m(6)A-Dependent Nuclear RNA Processing Events. Cell. 2015;162: 1299–1308. doi:10.1016/j.cell.2015.08.011

83. Coots RA, Liu X-M, Mao Y, Dong L, Zhou J, Wan J, et al. m6A Facilitates eIF4F-Independent mRNA Translation. Molecular Cell. 2017;68: 504–514.e7. doi:10.1016/j.molcel.2017.10.002

84. Zhou KI, Parisien M, Dai Q, Liu N, Diatchenko L, Sachleben JR, et al. N(6)-Methyladenosine Modification in a Long Noncoding RNA Hairpin Predisposes Its Conformation to Protein Binding. J Mol Biol. 2016;428: 822–833. doi:10.1016/j.jmb.2015.08.021

85. Lewis CJT, Pan T, Kalsotra A. RNA modifications and structures cooperate to guide RNA-protein interactions. Nat Rev Mol Cell Biol. 2017;18: 202–210. doi:10.1038/nrm.2016.163

86. Xiang Y, Laurent B, Hsu C-H, Nachtergaele S, Lu Z, Sheng W, et al. RNA m(6)A methylation regulates the ultraviolet-induced DNA damage response. Nature. 2017;543: 573–576. doi:10.1038/nature21671

87. Slobodin B, Han R, Calderone V, Vrielink JAFO, Loayza-Puch F, Elkon R, et al. Transcription Impacts the Efficiency of mRNA Translation via Co-transcriptional N6-adenosine Methylation. Cell. 2017;169: 326–337.e12. doi:10.1016/j.cell.2017.03.031

88. Kennedy EM, Bogerd HP, Kornepati AVR, Kang D, Ghoshal D, Marshall JB, et al. Posttranscriptional m(6)A Editing of HIV-1 mRNAs Enhances Viral Gene Expression. Cell Host Microbe. 2016;19: 675–685. doi:10.1016/j.chom.2016.04.002

89. Lichinchi G, Gao S, Saletore Y, Gonzalez GM, Bansal V, Wang Y, et al. Dynamics of the human and viral m(6)A RNA methylomes during HIV-1 infection of T cells. Nat Microbiol. 2016;1: 16011. doi:10.1038/nmicrobiol.2016.11

90. Gonzales-van Horn SR, Sarnow P. Making the Mark: The Role of Adenosine Modifications in the Life Cycle of RNA Viruses. Cell Host Microbe. 2017;21: 661–669. doi:10.1016/j.chom.2017.05.008

91. Tirumuru N, Zhao BS, Lu W, Lu Z, He C, Wu L. N(6)-methyladenosine of HIV-1 RNA regulates viral infection and HIV-1 Gag protein expression. Elife. 2016;5: 165. doi:10.7554/eLife.15528

92. Martínez-Pérez M, Aparicio F, López-Gresa MP, Bellés JM, Sánchez-Navarro JA, Pallás V. Arabidopsis m(6)A demethylase activity modulates viral infection of a plant virus and the m(6)A abundance in its genomic RNAs. Proc Natl Acad Sci USA. 2017. doi:10.1073/pnas.1703139114

93. Durbin AF, Wang C, Marcotrigiano J, Gehrke L. RNAs Containing Modified Nucleotides Fail To Trigger RIG-I Conformational Changes for Innate Immune Signaling. MBio. American Society for Microbiology; 2016;7: e00833–16. doi:10.1128/mBio.00833-16

94. Lavi S, Shatkin AJ. Methylated simian virus 40-specific RNA from nuclei and cytoplasm of infected BSC-1 cells. PNAS. National Acad Sciences; 1975;72: 2012–2016.

95. Krug RM, Morgan MA, Shatkin AJ. Influenza viral mRNA contains internal N6-methyladenosine and 5'-terminal 7-methylguanosine in cap structures. J Virol. 1976;20: 45–53. doi:10.1177/1091581816683642

96. Kahana C, Lavi S, Groner Y. Identification and mapping of N6 methyladenosine containing sequences in simian virus 40 RNA. Nucleic Acids Research. 1979;6: 2879–2899.

97. Moss B, Gershowitz A, Stringer JR, Holland LE, Wagner EK. 5'-Terminal and internal methylated nucleosides in herpes simplex virus type 1 mRNA. J Virol. American Society for Microbiology; 1977;23: 234–239.

98. Sommer S, Salditt-Georgieff M. The methylation of adenovirus-specific nuclear and cytoplasmic RNA. Nucleic Acids Research. 1976;3: 749–765.

99. Tsai K, Courtney DG, Cullen BR. Addition of m6A to SV40 late mRNAs enhances viral structural gene expression and replication. Flemington EK, editor. PLoS Pathog. 2018;14: e1006919. doi:10.1371/journal.ppat.1006919

100. Vieira J, O'Hearn PM. Use of the red fluorescent protein as a marker of Kaposi's sarcoma-associated herpesvirus lytic gene expression. Virology. 2004;325: 225–240. doi:10.1016/j.virol.2004.03.049

101. Myoung J, Ganem D. Infection of Lymphoblastoid Cell Lines by Kaposi's Sarcoma-Associated Herpesvirus: Critical Role of Cell-Associated Virus. J Virol. 2011;85: 9767–9777. doi:10.1128/JVI.05136-11

102. Sun R, Lin SF, Gradoville L, Miller G. Polyadenylylated nuclear RNA encoded by Kaposi sarcoma-associated herpesvirus. PNAS. National Academy of Sciences; 1996;93: 11883–11888.

103. Bai Z, Huang Y, Li W, Zhu Y, Jung JU, Lu C, et al. Genomewide mapping and screening of Kaposi“s sarcoma-associated herpesvirus (KSHV) 3” untranslated regions identify bicistronic and polycistronic viral transcripts as frequent targets of KSHV microRNAs. J Virol. American Society for Microbiology; 2014;88: 377–392. doi:10.1128/JVI.02689-13

104. Chandriani S, Ganem D. Array-based transcript profiling and limiting-dilution reverse transcription-PCR analysis identify additional latent genes in Kaposi's sarcoma-associated herpesvirus. J Virol. American Society for Microbiology; 2010;84: 5565–5573. doi:10.1128/JVI.02723-09

105. Lukac DM, Kirshner JR, Ganem D. Transcriptional activation by the product of open reading frame 50 of Kaposi's sarcoma-associated herpesvirus is required for lytic viral reactivation in B cells. J Virol. 1999;73: 9348–9361.

106. Ke S, Pandya-Jones A, Saito Y, Fak JJ, Vågbø CB, Geula S, et al. m(6)A mRNA modifications are deposited in nascent pre-mRNA and are not required for splicing but do specify cytoplasmic turnover. Genes Dev. Cold Spring Harbor Lab; 2017;31: 990–1006. doi:10.1101/gad.301036.117

107. Cleary MD, Meiering CD, Jan E, Guymon R, Boothroyd JC. Biosynthetic labeling of RNA with uracil phosphoribosyltransferase allows cell-specific microarray analysis of mRNA synthesis and decay. Nat Biotechnol. 2005;23: 232–237. doi:10.1038/nbt1061

108. Woodford TA, Schlegel R, Pardee AB. Selective isolation of newly synthesized mammalian mRNA after in vivo labeling with 4-thiouridine or 6-thioguanosine. Analytical biochemistry. 1988;171: 166–172. doi:10.1016/0003-2697(88)90138-8

109. Brulois KF, Chang H, Lee AS-Y, Ensser A, Wong L-Y, Toth Z, et al. Construction and manipulation of a new Kaposi's sarcoma-associated herpesvirus bacterial artificial chromosome clone. J Virol. 2012;86: 9708–9720. doi:10.1128/JVI.01019-12

110. Nakamura H, Lu M, Gwack Y, Souvlis J, Zeichner SL, Jung JU. Global Changes in Kaposi's Sarcoma-Associated Virus Gene Expression Patterns following Expression of a Tetracycline-Inducible Rta Transactivator. J Virol. 2003;77: 4205–4220. doi:10.1128/JVI.77.7.4205-4220.2003

111. Tan B, Liu H, Zhang S, da Silva SR, Zhang L, Meng J, et al. Viral and cellular N6-methyladenosine and N6,2'-O-dimethyladenosine epitranscriptomes in the KSHV life cycle. Nat Microbiol. 2018;3: 108–120. doi:10.1038/s41564-017-0056-8

112. Wu R, Jiang D, Wang Y, Wang X. N (6)-Methyladenosine (m(6)A) Methylation in mRNA with A Dynamic and Reversible Epigenetic Modification. Mol Biotechnol. Springer US; 2016;58: 450–459. doi:10.1007/s12033-016-9947-9

113. Fry NJ, Law BA, Ilkayeva OR, Holley CL, Mansfield KD. N(6)-methyladenosine is required for the hypoxic stabilization of specific mRNAs. RNA. Cold Spring Harbor Lab; 2017;23: 1444–1455. doi:10.1261/rna.061044.117

114. Abernathy E, Gilbertson S, Alla R, Glaunsinger B. Viral Nucleases Induce an mRNA Degradation- Transcription Feedback Loop in Mammalian Cells. Cell Host Microbe. Elsevier Inc; 2015;18: 243–253. doi:10.1016/j.chom.2015.06.019

115. Dominissini D, Moshitch-Moshkovitz S, Salmon-Divon M, Amariglio N, Rechavi G. Transcriptome-wide mapping of N(6)-methyladenosine by m(6)A-seq based on immunocapturing and massively parallel sequencing. Nat Protoc. 2013;8: 176–189. doi:10.1038/nprot.2012.148

116. Arias C, Weisburd B, Stern-Ginossar N, Mercier A, Madrid AS, Bellare P, et al. KSHV 2.0: a comprehensive annotation of the Kaposi's sarcoma-associated herpesvirus genome using next-generation sequencing reveals novel genomic and functional features. PLoS Pathog. 2014;10: e1003847. doi:10.1371/journal.ppat.1003847

117. Brocard M, Ruggieri A, Locker N. m6A RNA methylation, a new hallmark in virus-host interactions. J Gen Virol. 2017;98: 2207–2214. doi:10.1099/jgv.0.000910

118. Kennedy EM, Courtney DG, Tsai K, Cullen BR. Viral Epitranscriptomics. Sullivan CS, editor. J Virol. American Society for Microbiology Journals; 2017;91: 127. doi:10.1128/JVI.02263-16

119. Goff SP. Host factors exploited by retroviruses. Nature Reviews Microbiology. Nature Publishing Group; 2007;5: 253–263. doi:10.1038/nrmicro1541

120. Caballero A, Tabernero D, Buti M, Rodriguez-Frias F. Hepatitis B virus: The challenge of an ancient virus with multiple faces and a remarkable replication strategy. Antiviral Res. 2018;158: 34–44. doi:10.1016/j.antiviral.2018.07.019

121. Grozhik AV, Linder B, Olarerin-George AO, Jaffrey SR. Mapping m6A at Individual-Nucleotide Resolution Using Crosslinking and Immunoprecipitation (miCLIP). Methods Mol Biol. New York, NY: Springer New York; 2017;1562: 55–78. doi:10.1007/978-1-4939-6807-7_5

122. Yu F, Harada JN, Brown HJ, Deng H, Song MJ, Wu T-T, et al. Systematic Identification of Cellular Signals Reactivating Kaposi Sarcoma–Associated Herpesvirus. PLoS Pathog. 2007;3: e44–12. doi:10.1371/journal.ppat.0030044

123. Ivashkiv LB, Donlin LT. Regulation of type I interferon responses. Nat Rev

Immunol. Nature Publishing Group; 2014;14: 36–49. doi:10.1038/nri3581

124. Savan R. Post-transcriptional regulation of interferons and their signaling pathways. J Interferon Cytokine Res. Mary Ann Liebert, Inc. 140 Huguenot Street, 3rd Floor New Rochelle, NY 10801 USA; 2014;34: 318–329. doi:10.1089/jir.2013.0117

125. Winkler R, Abram E, Lasman L, Geula S, Soyris C, Nachshon A, et al. m6A mRNA methylation controls the innate immune response to infection by targeting type I interferons. Nature Immunology. 2018.

126. Rubio RM, Depledge DP, Bianco C, Thompson L, Mohr I. RNA m6A modification enzymes shape innate responses to DNA by regulating interferon β. Genes Dev. 2018. doi:10.1101/gad.319475.118

127. Hesser CR, Karijolich J, Dominissini D, He C, Glaunsinger BA. N6-methyladenosine modification and the YTHDF2 reader protein play cell type specific roles in lytic viral gene expression during Kaposi's sarcoma-associated herpesvirus infection. Dittmer DP, editor. PLoS Pathog. 2018;14: e1006995. doi:10.1371/journal.ppat.1006995